

Cross-correlating Sunyaev-Zel'dovich and Weak Lensing Maps

Dipak Munshi¹, Shahab Joudaki², Peter Coles¹, Joseph Smidt²

¹*School of Physics and Astronomy, Cardiff University, Queen's Buildings, 5 The Parade, Cardiff, CF24 3AA, UK*

²*Department of Physics and Astronomy, University of California, Irvine, CA 92697*

23 November 2011, Revision: 0.9

ABSTRACT

We present novel statistical tools to cross-correlate frequency cleaned thermal Sunyaev-Zel'dovich (tSZ) maps and tomographic weak lensing (wl) convergence maps. Moving beyond the lowest order cross-correlation, we introduce a hierarchy of mixed higher-order statistics, the cumulants and cumulant correlators, to analyze non-Gaussianity in real space, as well as corresponding polyspectra in the harmonic domain. Using these moments, we derive analytical expressions for the joint two-point probability distribution function (2PDF) for smoothed tSZ (y_s) and convergence (κ_s) maps. The presence of tomographic information allows us to study the evolution of higher order *mixed* tSZ-weak lensing statistics with redshift. We express the *joint* PDFs $p_{\kappa y}(\kappa_s, y_s)$ in terms of individual one-point PDFs ($p_{\kappa}(\kappa_s)$, $p_y(y_s)$) and the relevant bias functions ($b_{\kappa}(\kappa_s)$, $b_y(y_s)$). Analytical results for two different regimes are presented that correspond to the small and large angular smoothing scales. Results are also obtained for corresponding *hot spots* in the tSZ and convergence maps. In addition to results based on hierarchical techniques and perturbative methods, we present results of calculations based on the lognormal approximation. The analytical expressions derived here are generic and applicable to cross-correlation studies of arbitrary tracers of large scale structure including e.g. that of tSZ and soft X-ray background.

Key words: : Cosmology – Weak lensing Surveys – Sunyaev-Zel'dovich Surveys – Methods: analytical, statistical, numerical

1 INTRODUCTION

Free electrons in the Universe can be detected through the inverse Compton scattering of Cosmic Microwave Background (CMB) photons (Sunyaev & Zeldovich 1980, 1972; Birkinshaw 1999; Rephaeli 1995). An inhomogeneous distribution of electrons thus induces a secondary anisotropy in the CMB radiation, which is proportional to the thermal energy of the electrons integrated along the line of sight direction. This well-known effect is called the thermal Sunyaev-Zel'dovich effect (tSZ) and it is now routinely being used to image nearby galaxy clusters (Reese et al. 2002; Jones et al. 2005; LaRoque 2006) which the electron temperature can reach the order of 10keV. The future seems set for a huge increase in Sunyaev-Zel'dovich measurements of galaxy clusters; early data from Planck alone has generated 189 candidates with reasonably high signal-to-noise ratios (Planck Collaboration 2011). In the intergalactic medium (IGM), however, the gas is expected to be in mildly overdense regions and to reach a temperature of only 1keV or so. While the tSZ effect from clusters can alter the temperature of the CMB by an amount of order of mK in the Rayleigh-Jeans part of the spectrum, the contribution from the IGM is expected only to reach the μ K range. This is below the threshold for detection by WMAP, but should nevertheless be detectable by the ongoing Planck Surveyor¹ due to its wider frequency coverage, higher sensitivity, and improved resolution (Hansen et al. 2005; Joudaki et al. 2010).

The unique spectral dependence of the tSZ effect helps in the task of separating it from other sources of CMB temperature fluctuations so various well developed component separation schemes are available for construction of frequency-cleaned SZ maps (Leach 2008; Bouchet & Gispert 1999; Delabroullie, Cardoso & Patanchon 2003). The construction of such maps will provide us with a direct opportunity to probe the thermal history of the Universe, in tandem with other observations: owing to their thermal (peculiar motions) ionized electrons scatter CMB photons, an effect which can be studied using the tSZ effect (Rosati, Borgani & Norman 1998); the neutral component of the IGM can be also be probed via observations of the Lyman- α forest (Rauch 1998); X-ray emission due to the thermal bremsstrahlung that originates from the interaction of

¹ <http://www.rssd.esa.int/index.php?project=SP>

ionized electrons and nuclei can also provide clues to the nature and evolution of the IGM. These tracers all probe different phases of the IGM and thus play complementary roles. For example, the X-ray emission depends on the square of the density, so is most sensitive to the densest regions in the IGM, primarily in the local Universe, while tSZ studies can probe the more distant Universe because Compton scattering is independent of redshift, as well as being an unbiased tracer of all electrons, as they all participate in the scattering, the tSZ effect is weakly dependent on density so probes the electron density in a wide range of environments.

The modeling of lower order statistics of the tSZ effect can be carried out using various approaches. In the past (Seljak 2000; Zhang & Pen 2001; Komatsu & Seljak 2001; Zhang & Seth 2007; Cooray 2000, 2001) the modeling has followed the halo model (Cooray & Seth 2002). The statistical distribution of haloes, specifically their number-density as a function of mass (i.e. their mass function), is assumed to be that predicted provided by the Press-Schechter formalism (Press & Schechter 1974) or its generalisations, and the radial profile of such haloes were assumed to be that of Navarro, Frenk & White (1996). The hot gas, assumed to have been heated by shocks, is taken to be in hydrodynamical equilibrium with the dark matter distribution. The typical temperature reached in such systems is sufficient to ionize the hydrogen and helium atoms. These ingredients are sufficient to model the tSZ effect raising from collapsed haloes (Cooray 2000); in addition to this analytical modeling, numerical simulation of the tSZ plays an important role in our understanding of the physics involved (Persi et al. 1995; Refregier et al. 2000; Seljak et al. 2001; Springel et al. 2001; White, Hernquist & Springel 2002; Lin et al. 2004; Zhang, Pen & Trac 2004; Cao, Liu & Fang 2007; Roncarelli et al. 2007; Hallman et al. 2009, 2007; da Silva et al. 2000). To extend the halo model to larger scales, the extended distribution of free electrons is typically assumed to trace the distribution of dark matter on large scales where the variations in density are in the linear or quasi-linear regime. A perturbative approach along these lines has been developed by several authors over the years (Cooray 2000, 2001; Cooray & Hu 2000; Goldberg & Spergel 1999a,b; Munshi et al. 2011a,b).

Ongoing and proposed ground surveys such as SZA², ACT³, APEX⁴, SPT⁵ and the ongoing all sky survey Planck will map the γ -sky with a great precision. The SPT (Lueker et al. 2010) collaboration has already reported the measurement of the tSZ power spectrum at $l \approx 3000$; the ACT (Fowler et al. 2010; Dunkley et al. 2010) collaboration has also reported analysis on similar scales. It is expected that ongoing surveys will improve these measurements due to their improved sky coverage as well as wider frequency range. It is important to realize why the study of secondaries such as tSZ should be an important aspect of any CMB mission. In addition to the important physics the secondaries probe, accurate modeling of the secondary non-Gaussianities is required to avoid 20% – 30% constraint degradations in future CMB data-sets such as Planck and CMBPol⁶ (Smidt et al. 2010).

While the tSZ surveys described above provide a direct probe of the baryonic Universe, weak lensing observations (Munshi et al. 2008) on the other hand can map the dark matter distribution in an unbiased way. In recent years there has been tremendous progress on the technical front in terms of specification and control of systematics in weak lensing observables. There are many ongoing and future weak lensing surveys such as CFHT⁷ legacy survey, Pan-STARRS⁸ and the Dark Energy survey (DES)⁹ and in future, the Large Synoptic Survey Telescope (LSST)¹⁰, Joint Dark Energy Mission (JDEM)¹¹ will map the dark matter and dark energy distribution of the entire sky in unprecedented details. Among other things, hold great promise in shedding light on the nature of the dark energy and the origin of neutrino masses (Joudaki & Kaplinghat 2011), where the weak lensing signals dominate the others considered by e.g. the Dark Energy Task Force (Albrecht et al. 2011). However, the optimism associated with lensing is predicated on overcoming the vast systematic uncertainties in both measurement and in theory (Hirata & Seljak 2004; Ma, Hu & Huterer 2005; Cooray & Hu 2002; Hirata & Seljak 2003; White 2004; Huterer 2006; McDonald, Trac & Contaldi 2006). The statistics of the weak lensing convergence have been studied in great detail using an extension of perturbation theory (Munshi & Jain 2000, 2001; Munshi, Valageas & Barber 2004) and methods based on the halo model (Cooray & Hu 2000; Takada & Jain 2002, 2003). These studies developed techniques that can be used to predict the lower-order moments (equivalent to the power spectrum and multi-spectra in the harmonic domain) and the entire PDF for a given weak lensing survey. The photometric redshifts of source galaxies are useful for tomographic studies of the dark matter distribution and establish a three-dimensional picture of their distribution (Munshi et al. 2010).

Due to the line of sight integration inherent in the tSZ effect, the redshift evolution is completely lost which degrades the power of tSZ to distinguish different thermal histories. It is however possible to recover some of the information lost by cross-correlating the tSZ with external tracers (Shao et al. 2011a; Zhang & Pen 2001). These tracers could comprise galaxy surveys with spectroscopic redshift information or dark matter distribution from weak lensing surveys in tomographic slices. Such cross-correlations has been studied using two-point statistics. We extend these results to higher order. Higher order statistics such as cumulants and cumulant correlators (Munshi, Melott & Coles 1999) can probe higher order cross-correlations and can in principle provide an independent probe of the bias associated with the baryonic pressure fluctuations. The tomographic

² <http://astro.uchicago.edu/sza>

³ <http://www.physics.princeton.edu/act>

⁴ <http://bolo.berkeley.edu/apexsz>

⁵ <http://pole.uchicago.edu>

⁶ <http://cmbpol.uchicago.edu/>

⁷ <http://www.cfht.hawaii.edu/Sciences/CFHLS/>

⁸ <http://pan-starrs.ifa.hawaii.edu/>

⁹ <https://www.darkenergysurvey.org/>

¹⁰ http://www.lsst.org/llst_home.shtml

¹¹ <http://jdem.gsfc.nasa.gov/>

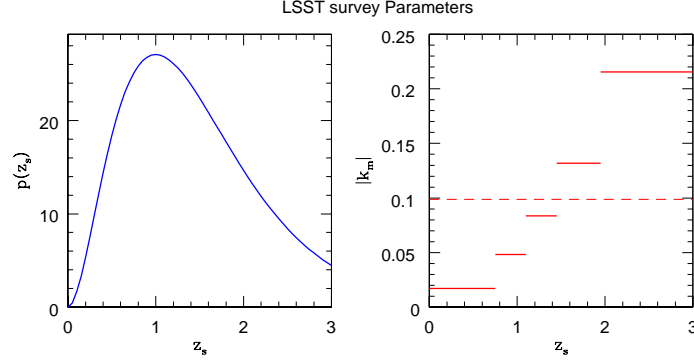


Figure 1. The parameter κ_m , that denotes the minimum value of convergence is displayed as a function of source redshift for the Λ CDM cosmology (right panel). The parameter κ_m is independent of angular smoothing scale. The dashed line in the right panel corresponds to κ_m for the projected 2D survey. The left panel shows the source distribution as a function of redshift.

cross-correlation statistics that we develop here can be applied to surveys with overlapping sky coverage. Many of the weak lensing surveys and the tSZ surveys will have overlapping sky coverage. For example, DES will have overlap with the SPT sky coverage and plans to measure photometric redshifts of roughly 10^8 galaxies up to $z = 1.3$. Tomographic cross-correlation statistics at second or higher-order can provide a more detailed picture of the evolution of the thermal history of the baryonic gas by mapping the associated pressure fluctuation. The results presented here are generic and can be extended to study other secondaries, such as the cross-correlation involving CMB lensing and tSZ maps.

This paper is organized as follows. In §2 we introduce our notations for both tSZ and weak-lensing observables. Next we introduce the mixed cumulant correlators and the cumulants in §3. Two different models are used to model the underlying dark matter distribution. We employ the (Smith et al. 2003) prescription, for modelling the evolution of matter power spectrum and use the hierarchical approach for modelling of the higher order correlation hierarchy. This allows us to extend the lower order moment results to arbitrary order and construct the relevant PDF and bias for the smoothed weak lensing κ field and the y maps in §4. A brief review of the hierarchical ansatz in the quasilinear and non-linear regimes, as well as the lognormal approach, is provided in the appendix.

2 NOTATIONS

In this section, we introduce our notation for the tSZ effect and weak lensing convergence. We will use the following line element:

$$ds^2 = -c^2 dt^2 + a^2(r) [dr^2 + d_A^2(r)(\sin^2 \theta d\theta^2 + d\phi^2)] \quad (1)$$

Here $d_A(r)$ is the comoving angular diameter distance at a (comoving) radial distance r . The angular diameter distance is $d_A(r) = (-K)^{-1/2} \sinh((-K)^{1/2} r)$ for negative curvature, $d_A(r) = (K)^{-1/2} \sin((K)^{1/2} r)$ for positive curvature, and for a flat Universe $d_A(r) = r$. The parameters H_0 and Ω_0 decide the constant K : $K = (\Omega_0 - 1)H_0^2$. The underlying cosmology that we adopt for numerical study is specified by the following parameter values (to be introduced later): $\Omega_\Lambda = 0.741$, $h = 0.72$, $\Omega_b = 0.044$, $\Omega_{\text{CDM}} = 0.215$, $\Omega_0 = \Omega_b + \Omega_{\text{CDM}}$, $n_s = 0.964$, $w_0 = -1$, $w_a = 0$, $\sigma_8 = 0.803$, $\Omega_\nu = 0$. The comoving radial distance at a redshift z is determined by the cosmology (Ω_0, H_0)

$$r(z) = \int_0^z \frac{dz}{H_0 \sqrt{\Omega_0(1+z)^3 + \Omega_K(1+z)^2 + \Omega_\Lambda}} \quad (2)$$

Throughout, c will denote the speed of light and will be set to unity.

2.1 Thermal Sunyaev Zel'dovich Effect

The tSZ effect contributes to the CMB temperature fluctuation and is typically expressed as $\delta_T(\nu, \hat{\Omega}) = \Delta T(\hat{\Omega})/T_0 = g(x_\nu)y(\hat{\Omega})$. In this expression, $g(x_\nu)$ corresponds to the spectral dependence and $y(\hat{\Omega})$ encodes the angular dependence; x_ν represents the dimensionless frequency and $\hat{\Omega} = (\theta, \phi)$ corresponds to a unit vector that signifies pixel positions. A subscript s will be used to denote the smoothed maps, e.g. $y_s(\hat{\Omega})$. In the non-relativistic limit $g(x_\nu)$ takes the following form:

$$g(x_\nu) = x_\nu \coth\left(\frac{x_\nu}{2}\right) - 4 = \left(x_\nu \frac{e^{x_\nu} + 1}{e^{x_\nu} - 1} - 4\right); \quad x_\nu = \frac{h\nu}{k_B T_0} = \frac{\nu}{56.84 \text{GHz}} = \frac{5.28 \text{mm}}{\lambda}; \quad (3)$$

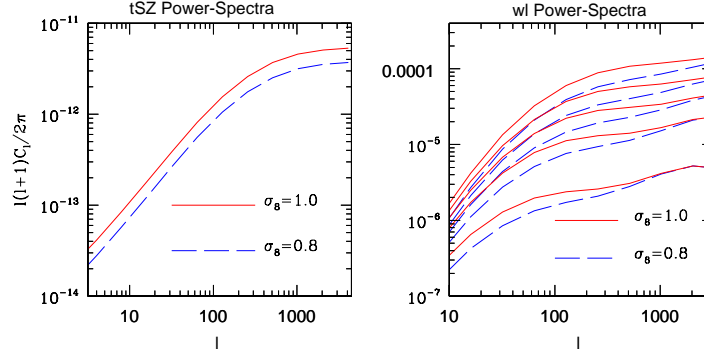


Figure 2. The left panel shows tSZ power spectrum as a function of the harmonics l . The right panel shows redshift-resolved tomographic weak lensing and tSZ cross-spectra as function of l . The background cosmology is assumed Λ CDM. The solid lines in each panel correspond to $\sigma_8 = 1$ and the dashed lines correspond to $\sigma_8 = 0.8$.

Here k_B and h are the Boltzmann and Planck constants respectively; ν denotes the frequency of the photon and $T_0 = 2.726$ K is the temperature of the CMB sky. The tSZ effect shows as CMB temperature decrement at $\nu \ll 218$ GHz and as an increment at $\nu \gg 218$ GHz, with a null at $\nu = 218$ GHz. In the Rayleigh Jeans limit, characterized by $x \ll 1$, $g(x) \approx -2$ is roughly independent of frequency and in the other limiting situation $x \gg 1$, $g(x_\nu) \approx (x_\nu - 4)$. The key information regarding thermal history of the Universe is encoded in $y(\hat{\Omega})$ maps that are extracted from frequency maps obtained through multifrequency CMB observations. The y maps are opacity weighted integrated pressure fluctuations along the line of sight.

$$y(\hat{\Omega}) \equiv \int ds n_e \sigma_T \frac{k_B T_e}{m_e c^2} = \frac{\sigma_T}{m_e c^2} \int_0^{r_H} dr a(r) n_e k_B T_e(\hat{\Omega}, r) = \frac{\sigma_T}{m_e c^2} \int_0^{\eta_H} d\eta a(\eta) \Pi_e(\eta, \hat{\Omega}) = \int_0^{r_H} dr w_{SZ}(r) \pi_e(r). \quad (4)$$

Here $\Pi_e = n_e k_B T_e$, while m_e corresponds to the electron mass, k_B denotes the Boltzmann's constant, $\sigma_T = 6.6510^{-25} \text{ cm}^2$ represents the Thompson cross-section, n_e denotes the number-density of electrons, and T_e is the electron temperature. Conformal time is denoted by $d\eta = dt/a(t)$. The line-of-sight integral depends on the comoving radial coordinate distance r and $a(r)$ is the corresponding scale factor of the Universe. The weight is defined as $w_{SZ}(r) = \dot{r}(r) = \sigma_T n_e(r) a(r)$, where the dot defines the derivative with respect to comoving radial distance r , and the 3D pressure fluctuation is defined as $\pi_e = k_B T_e / m_e c^2$. We will cross-correlate the comptonization map $y(\hat{\Omega})$ with tomographic and projected maps from weak lensing surveys to constrain the thermal history of the Universe and its evolution with redshift. Throughout, we will consider the Rayleigh-Jeans part of the spectrum $\delta_T = -2y$; for ACT and SPT operating at $\nu = 150$ GHz from Eq. (3) we get $g(x) = -0.95$. Detailed modelling of the bias is required only for the computation of variance. The variance $\langle \delta y^2(\hat{\Omega}) \rangle$ samples the pressure fluctuation power spectrum $P_{\pi\pi}$ and is expressed as:

$$\langle \delta y^2(\hat{\Omega}) \rangle_c = \int_0^{r_H} dr \frac{\omega_{SZ}^2(r)}{d_A^2(r)} \int \frac{d^2 l}{(2\pi)^2} P_{\pi\pi} \left[\frac{l}{d_A(r)}, r \right] b_l^2(\theta_s). \quad (5)$$

The pressure power spectrum $P_{\pi\pi}(k, z)$ at a redshift z is expressed in terms of the underlying power spectrum $P_{\delta\delta}(k, z)$ using a bias $b_\pi(k, z)$, i.e. $P_{\pi\pi}(k, z) = b^2(k, z) P_{\delta\delta}(k, z)$. The bias $b_\pi(k, z)$ is assumed to be independent of length scale or equivalently wave number k , i.e. $b_\pi(k, z) = b_\pi(z)$. The redshift dependent bias can be expressed as $b_\pi(z) = b_\pi(0)/(1+z)$. Here $b_\pi(0)$ can be written as $b_\pi(0) = k_B T_e(0) b_\delta / m_e c^2$. Different values of b_δ have been reported, e.g. (Refregier et al. 2000) found $b_\delta \approx 8 - 9$ and $T_e(0) \approx 0.3 - 0.4$. On the other hand (Seljak et al. 2001) found $b_\delta \approx 3 - 4$. Typical value of $b_\pi(0)$ found by (Cen & Ostriker 1999) is $b_\pi(0) = 0.0039$. This is a factor of two lower than the value used by (Goldberg & Spergel 1999a,b) and (Cooray & Hu 2000). A Gaussian beam $b_l(\theta_s)$ with FWHM at θ_s is assumed. The PDF and bias functions of hot-spots are specified in terms of the normalized cumulants or cumulant correlators, which we probe next.

2.2 Weak Lensing in Projection and Tomography

Cosmological weak lensing effects are conveniently encoded in the effective convergence field, which is defined as a weighted projection of the matter density contrast δ . The statistics of the smoothed weak lensing convergence κ_s are similar to the projected 3D density contrast $\delta(\mathbf{x})$ and can be expressed through a line of sight integration $\kappa(\hat{\Omega}) = \int_0^{r_s} dr w_{wl}(r) \delta(r, \hat{\Omega})$. Their weight $w_{wl}(r)$ is sensitive to the source distribution; for 2D surveys without any source redshift information, can be expressed as

$$w_{wl}(r) = \frac{3}{2} \frac{H_0^2}{c^2} \Omega_M a^{-1}(r) d_A(r) \int_r^{r_s} dr p_s(r) \frac{dz_s}{dr_s} \frac{d_A(r - r_s)}{d(r_s)}; \quad p_s(z_s) = \bar{n}_g \frac{z_s^2}{2z_0^3} \exp^{-z_s/z_0}. \quad (6)$$

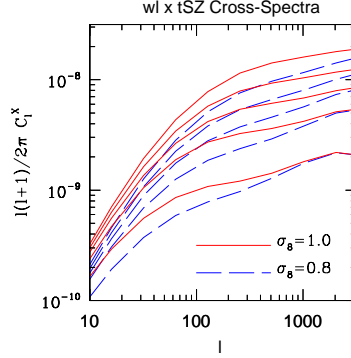


Figure 3. The redshift-resolved cross spectra $C_l^{(i)\kappa,y}$ given in Eq. (12) for weak lensing tomographic slices and the tSZ survey are plotted as function of harmonics l .

Here $p_s(z_s)$ represents the source redshift distribution. The peak of the distribution is reached at $2z_0$. We will adopt two different survey configurations. We adopt $z_0 = 0.5$ for the LSST survey. For the tomographic calculation we divide the entire source redshift range in five redshift bins with each tomographic bin containing roughly the same number density of source galaxies. The redshift bins of the sources are delimited at $[0.75, 1.1, 1.45, 1.95, 3.00]$. The tomographic convergence maps $\kappa^{(i)}(\hat{\Omega}) = \int_0^{r_s} dr w_{wl}^{(i)}(r) \delta(r, \hat{\Omega})$ depend on individual weights:

$$w_{wl}^{(i)}(r) = \frac{3}{2} \frac{H_0^2}{c^2} \Omega_M \frac{1}{\bar{n}_i} a^{-1}(r) d_A(r) \int_{\max\{r, r_i\}}^{r_{i+1}} dr p_s(r) \frac{dz_s}{dr_s} \frac{d_A(r - r_s)}{d(r_s)}. \quad (7)$$

The projected convergences for individual tomographic bins are defined as $\kappa_m^{(i)} = - \int_0^{r_s} dr w_{wl}^{(i)}(r)$. We will next use these expressions to derive the cross-correlations at second- and higher-order both in real space and the harmonic domain.

Some comments are in order at this point. The hierarchical model that we use here was previously used by Zhang, Pen & Wang (2002); Cooray, Tegmark & Hu (2000); Cooray (2000, 2001). It is known that the y_s -parameter is proportional to the square of the density contrast δ^2 , so e.g. the three-point correlation function of y_s effectively samples the six-point correlation function of the underlying density contrast δ . However, studies by (Cooray 2000, 2001) assumed a linear biasing model for the pressure fluctuations, i.e. in the Fourier domain $\delta_\pi(k, z) = \delta(k, z) b_\pi(k, z)$. The pressure bias model assumes the pressure to be a linear convolution over the density field. Finally Cooray (2000, 2001) further simplified the bias $b_\pi(k, z)$ by factorizing it into a redshift dependent and momentum k dependent part. The spatial dependence was assumed to be constant. This is the simplification that we will use in our results, which will be useful in computation of correlation hierarchy to an arbitrary order. The hierarchical ansatz and the resulting scaling functions were also used by (Valageas, Schaefer & Silk 2001; Valageas & Silk 1999; Valageas & Schaeffer 2000). For computation of the number density of collapsed objects these were then used to obtain the thermal Sunyaev-Zel'dovich (tSZ) and kinetic Sunyaev-Zel'dovich (kSZ) effect statistics. The results derived here are complementary to calculations based on the halo model and are applicable to tSZ effect originating from the extragalactic ionized medium.

3 MIXED LOWER ORDER MOMENTS: CUMULANTS AND CUMULANT CORRELATORS

In this section, we present results in real space and in the harmonic domain that are completely generic and can provide useful information to study the pressure fluctuations in the baryonic gas. We apply these results to understand the studies involving tomographic bins from weak lensing surveys. In case of CMB lensing one of the source planes is identified with the last scattering surface. The cross-spectra $P_{\delta\pi}$ (defined below) can be probed by cross-correlating tomographic weak lensing maps $\kappa_{(i)}$ and the tSZ y maps of projected pressure fluctuations. These correlations sample the three dimensional density-pressure cross-spectra $P_{\delta\pi}$; using the small angle approximation (Kaiser 1998) one can write:

$$\langle \kappa_{(i)}(\hat{\Omega}_1) \delta y_s(\hat{\Omega}_2) \rangle_c = \int_0^{r_H} dr \frac{\omega_{(i)}(r) \omega_{SZ}(r)}{d_A^2(r)} \int \frac{d^2 \mathbf{l}}{(2\pi)^2} \exp(i\theta_{12} \cdot \mathbf{l}) P_{\delta\pi} \left[\frac{l}{d_A(r)}, r \right] b_l(\theta_s) W_{TH}(l\theta_s); \quad P_{\pi\delta}(k, z) = b_\pi(z) P_\delta(k, z). \quad (8)$$

Here $b_l(\theta_s)$ and $W_{TH}(l\theta_s) = (2J_1(l\theta_s)/l\theta_s)$ are Gaussian and Top-hat windows respectively. The line-of-sight directions $\hat{\Omega}_1$ and $\hat{\Omega}_2$ are separated by an angle θ_{12} . In our notation $|\mathbf{l}| = l$. The weight function $\omega_{(i)}(r)$ for tomographic convergence and $\omega_{SZ}(r)$ for tSZ surveys are defined in Eq. (7) and Eq. (4) respectively.

To study non-Gaussianity in pressure fluctuation we need to go beyond the power spectrum analysis; we propose the mixed cumulant correlators for this purpose. Cumulant correlators have the advantage of being very simple to estimate, and are defined in real space so can be useful

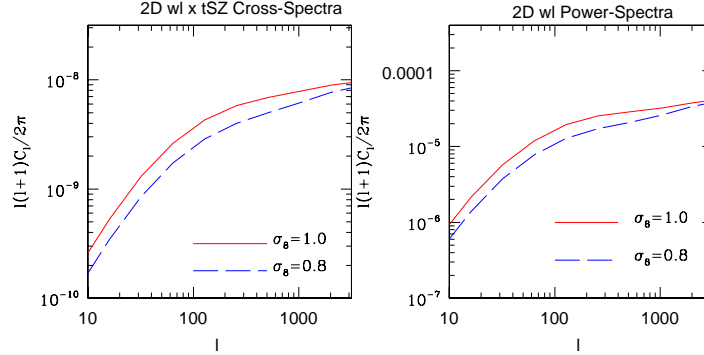


Figure 4. The projected (or 2D) weak lensing and tSZ cross-spectra is plotted as a function of harmonics l (left panel). We also show the projected weak lensing convergence power spectra as a function of l (right panel). Two different values of $\sigma_8 = [0.8, 1.0]$ are considered.

for smaller surveys. Similar results can be obtained for the kurt-spectra, which we will not consider here. We will consider a top-hat smoothing $W_{\text{TH}}(l\theta_s)$ for the convergence maps and a Gaussian beam $b_l(\theta_s)$ for the $y_s(\hat{\Omega})$ maps.

$$\langle \kappa_{(i)}^2(\hat{\Omega}_1) \delta y_s(\hat{\Omega}_2) \rangle_c = \int_0^{r_H} dr \frac{\omega_{(i)}^3(r) \omega_{\text{SZ}}(r)}{d_A^4(r)} \int \frac{d^2 \mathbf{l}_1}{(2\pi)^2} W_{\text{TH}}(l_1 \theta_s) \int \frac{d^2 \mathbf{l}_2}{(2\pi)^2} W_{\text{TH}}(l_2 \theta_s) \int \frac{d^2 \mathbf{l}_3}{(2\pi)^2} b_{l_3}(\theta_s) B_{\delta\delta\pi} \left(\frac{l_i}{d_A(r)}, r \right)_{\sum l_i=0} \quad (9)$$

$$\langle \kappa_{(i)}(\hat{\Omega}_1) \delta y_s^2(\hat{\Omega}_2) \rangle_c = \int_0^{r_H} dr \frac{\omega_{(i)}(r) \omega_{\text{SZ}}^2(r)}{d_A^4(r)} \int \frac{d^2 \mathbf{l}_1}{(2\pi)^2} W_{\text{TH}}(l_1 \theta_s) \int \frac{d^2 \mathbf{l}_2}{(2\pi)^2} b_{l_2}(\theta_s) \int \frac{d^2 \mathbf{l}_3}{(2\pi)^2} b_{l_3}(\theta_s) B_{\delta\pi\pi} \left(\frac{l_i}{d_A(r)}, r \right)_{\sum l_i=0} \quad (10)$$

Here $B_{\delta\delta\pi}$ represents the mixed bispectrum involving three dimensional density contrast $\delta(\mathbf{x})$ and pressure fluctuation $\pi(\mathbf{x})$. These *mixed* cumulant correlators should be considered in addition to the pure ones that probe $B_{\delta\delta\delta}$ and $B_{\pi\pi\pi}$. These results can trivially be extended to higher order to compute mixed cumulant correlators. At the level of fourth order they will probe the mixed trispectra of various types; e.g. we can use $\langle \kappa_{(i)}^2(\hat{\Omega}_1) y_s^2(\hat{\Omega}_2) \rangle_c$ $\langle \kappa_{(i)}^3(\hat{\Omega}_1) y_s(\hat{\Omega}_2) \rangle_c$ to probe the trispectra $T_{\delta\delta\pi\pi}$, $T_{\delta\delta\delta\pi}$ and $T_{\delta\pi\pi\pi}$. At these level these statistics are completely general and they can be estimated in real space simply by cross-correlating smoothed $y(\theta_s)$ and $\kappa(\theta_s)$ maps raised to suitable powers. The higher order expressions follow from the same logic.

The derivation so far has been completely generic. It does *not* depend on specific form of the multispectra. Later we will use a specific form for the correlation hierarchy which will allow us to include correlation functions to all order. This is done using a generating function formalism.

The results in the real space are suitable for smaller surveys. However with the increase in survey size it is pertinent to consider a harmonic space approach as real space measurements are often correlated. We will introduce power spectra in the harmonic domain that are Fourier transforms of the corresponding cumulant correlators in real space.

$$C_l^{\kappa\kappa,y} = \sum_{l_1 l_2} \sqrt{\frac{(2l_1+1)(2l_2+1)}{4\pi(2l+1)}} \begin{pmatrix} l_1 & l_2 & l \\ m_1 & m_2 & m \end{pmatrix} B_{l_1 l_2 l}^{\kappa\kappa y}; \quad C_l^{yy,\kappa} = \sum_{l_1 l_2} \sqrt{\frac{(2l_1+1)(2l_2+1)}{4\pi(2l+1)}} \begin{pmatrix} l_1 & l_2 & l \\ m_1 & m_2 & m \end{pmatrix} B_{l_1 l_2 l}^{yy\kappa}. \quad (11)$$

The skew- and kurt-spectra are simple to estimate from real data and the scatter for such estimates is well understood (Munshi & Heavens 2010; Munshi et al. 2011). These results can be used to construct a family of skew-spectra for various choices of tomographic slices. We also provide the expressions for the auto- and cross-spectra for tSZ and wl surveys below:

$$C_l^{(i)\kappa,y} = \int_0^{r_H} dr \frac{\omega_{(i)}(r) \omega_{\text{SZ}}(r)}{d_A^2(r)} P_{\delta\pi} \left(\frac{l_i}{d_A(r)}, r \right) \quad (12)$$

The auto spectra for wl and tSZ can be expressed in terms of $P_{\delta\delta}$ and $P_{\pi\pi}$ with suitable changes in the weight functions, i.e. $\omega_{(i)}^2(r)$ for wl surveys and $\omega_{\text{SZ}}^2(r)$ for tSZ surveys.

3.1 Hierarchical Ansatz

In deriving the above expressions we have not used any specific form for the matter correlation hierarchy, however the length scales involved in small angles are in the highly non-linear regime. Assuming a tree model for the matter correlation hierarchy in the highly non-linear regime one can write the most general case as (White 1979; Peebles 1983; Fry 1984; Bernardeau & Schaeffer 1992; Szapudi & Szalay 1993; Bernardeau &

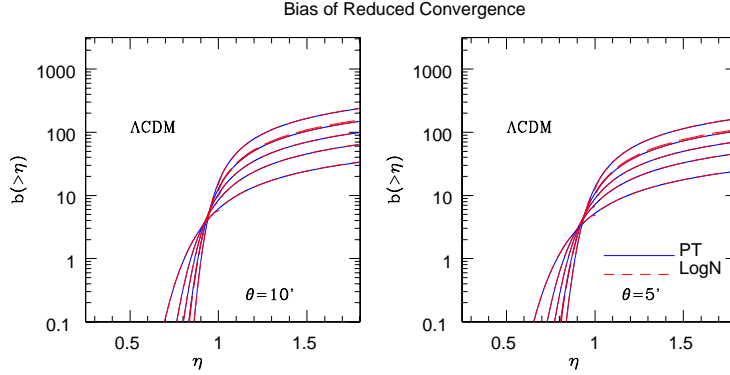


Figure 5. The bias function $b(\eta)$ of the reduced convergence is depicted for two different smoothing angular scales. The dashed lines show the analytical predictions from the hierarchical ansatz and the solid lines show predictions from the lognormal distribution. The left panel corresponds to $\theta_s = 10'$ and the right panel corresponds to $\theta_s = 5'$. The different curves in each panel correspond to different redshift bins. The lower curves correspond to shallower (lower redshift) bins and the higher curves correspond to deeper (higher redshift) bins. The top-most curve corresponds to the projected survey without any tomographic information.

Schaeffer 1999):

$$\xi_N^\delta(\mathbf{r}_1, \dots, \mathbf{r}_N) = \sum_{\alpha, N\text{-trees}} Q_{N,\alpha} \sum_{\text{labellings}} \prod_{\text{edges}(i,j)}^{(N-1)} \xi_2^\delta(\mathbf{r}_i, \mathbf{r}_j). \quad (13)$$

It is interesting to note that an exactly similar hierarchy develops in the quasi-linear regime in the limit of vanishing variance (Bernardeau 1992), however the hierarchical amplitudes $Q_{N,\alpha}$ become shape-dependent in such a case. In the highly nonlinear regime there are some indications that these functions become independent of shape parameters as has been suggested by studies of the lowest order parameter $Q_3 = Q$ using high resolution numerical simulations (Scocciamarro et al. 1998). In the Fourier space such an *ansatz* will mean that the whole hierarchy of multi-spectra B_δ, T_δ can be written in terms of sum of products of power-spectra P_δ , e.g. in low orders we can write:

$$B_\delta(\mathbf{k}_1, \mathbf{k}_2, \mathbf{k}_3)_{\sum k_i=0} = Q(P_\delta(k_1)P_\delta(k_2) + P_\delta(k_2)P_\delta(k_3) + P_\delta(k_3)P_\delta(k_1))\delta_D(\mathbf{k}_1 + \mathbf{k}_2 + \mathbf{k}_3), \quad (14)$$

$$T_\delta(\mathbf{k}_1, \mathbf{k}_2, \mathbf{k}_3, \mathbf{k}_4)_{\sum k_i=0} = [R_a P_\delta(k_1)P_\delta(|\mathbf{k}_1 + \mathbf{k}_2|)P_\delta(|\mathbf{k}_1 + \mathbf{k}_2 + \mathbf{k}_3|) + \text{cyc.perm.} \\ + R_b P_\delta(k_1)P_\delta(k_2)P_\delta(k_3) + \text{cyc.perm.}] \delta_D(\mathbf{k}_1 + \mathbf{k}_2 + \mathbf{k}_3 + \mathbf{k}_4) \quad (15)$$

Different hierarchical models differ in the way they predict the amplitudes of different tree topologies. Bernardeau & Schaeffer (1992) considered the case where amplitudes in general are factorizable, at each order one has a new “star” amplitude and higher order “snake” and “hybrid” amplitudes are constructed from lower order “star” amplitudes (see Munshi, Melott & Coles 1999a,b,c for a detailed description). In models proposed by Szapudi & Szalay (1993) it is assumed that all hierarchical amplitudes of a given order are actually degenerate. We do not use any of these specific models for clustering and only assume the hierarchical nature of the higher order correlation functions. In the past, primarily data from galaxy surveys have been analyzed extensively using these *ansatze*. Our main motivation here is to show that cross-correlation statistics of weak-lensing surveys and the tSZ surveys can also be analyzed using such techniques. The most general form for the lower order cumulant correlators in the large separation limit can be expressed as:

$$\langle \kappa_s^2(\hat{\Omega}_1) \delta y_s(\hat{\Omega}_2) \rangle_c = 2Q_3 \hat{C}_3[\mathcal{I}_{\theta_s} \mathcal{I}_{\theta_{12}}] = C_{21}^{\eta\eta'} \hat{C}_3[\mathcal{I}_{\theta_s} \mathcal{I}_{\theta_{12}}] \equiv C_{21}^{\kappa y} \langle \kappa_s^2 \rangle_c \langle \delta y_s(\hat{\Omega}_1) \kappa_s(\hat{\Omega}_2) \rangle_c, \quad (16)$$

$$\langle \kappa_s^3(\hat{\Omega}_1) \delta y_s(\hat{\Omega}_2) \rangle_c = (3R_a + 6R_b) \hat{C}_4[\mathcal{I}_{\theta_s}^2 \mathcal{I}_{\theta_{12}}] = C_{31}^{\eta\eta'} \hat{C}_4[\mathcal{I}_{\theta_s}^2 \mathcal{I}_{\theta_{12}}] \equiv C_{31}^{\kappa y} \langle \kappa_s^2 \rangle_c^2 \langle \kappa_s(\hat{\Omega}_1) \delta y_s(\hat{\Omega}_2) \rangle_c, \quad (17)$$

$$\langle \kappa_s^2(\hat{\Omega}_1) \delta y_s^2(\hat{\Omega}_2) \rangle_c = 4R_b \hat{C}_4[\mathcal{I}_{\theta_s} \mathcal{I}_{\theta_{12}}] = C_{22}^{\eta\eta'} \hat{C}_4[\mathcal{I}_{\theta_s} \mathcal{I}_{\theta_{12}}] \equiv C_{22}^{\kappa y} \langle \kappa_s^2 \rangle_c \langle \delta y_s^2 \rangle_c \langle \kappa_s(\hat{\Omega}_1) \delta y_s(\hat{\Omega}_2) \rangle_c, \quad (18)$$

$$\langle \kappa_s^4(\hat{\Omega}_1) \delta y_s(\hat{\Omega}_2) \rangle_c = (24S_a + 36S_b + 4S_c) \hat{C}_5[\mathcal{I}_{\theta_s}^3 \mathcal{I}_{\theta_{12}}] = C_{41}^{\eta\eta'} \hat{C}_5[\mathcal{I}_{\theta_s}^3 \mathcal{I}_{\theta_{12}}] \equiv C_{41}^{\kappa y} \langle \kappa_s^2 \rangle_c^3 \langle \kappa_s(\hat{\Omega}_1) \delta y_s(\hat{\Omega}_2) \rangle_c, \quad (19)$$

$$\langle \kappa_s^3(\hat{\Omega}_1) \delta y_s^2(\hat{\Omega}_2) \rangle_c = (12S_a + 6S_b) \hat{C}_5[\mathcal{I}_{\theta_s}^3 \mathcal{I}_{\theta_{12}}] = C_{32}^{\eta\eta'} \hat{C}_5[\mathcal{I}_{\theta_s}^3 \mathcal{I}_{\theta_{12}}] \equiv C_{32}^{\kappa y} \langle \kappa_s^2 \rangle_c^2 \langle \delta y_s^2 \rangle_c \langle \kappa_s(\hat{\Omega}_1) \delta y_s(\hat{\Omega}_2) \rangle_c. \quad (20)$$

Here $C_{pq}^{\kappa y}$ denotes the cumulant correlators of the convergence field and $C_{pq}^{\eta\eta'}$ denotes the cumulant correlators for the underlying mass distribution. The subscript c denotes the *connected* components of the higher order correlation functions. The amplitudes $R_a = \nu_2^2$, $R_b = \nu_3$ and $S_a = \nu_2^3$, $S_b = \nu_3\nu_2$, $S_c = \nu_4$ are expressed in terms of the vertices which can be evaluated using HEPT (Hyper Extended Perturbation Theory; Scocciamarro et al. (1998)). The exact expressions for various $C_{pq}^{\eta\eta'}$ presented in Eq. (20) are obtained by counting of the relevant tree diagrams. In

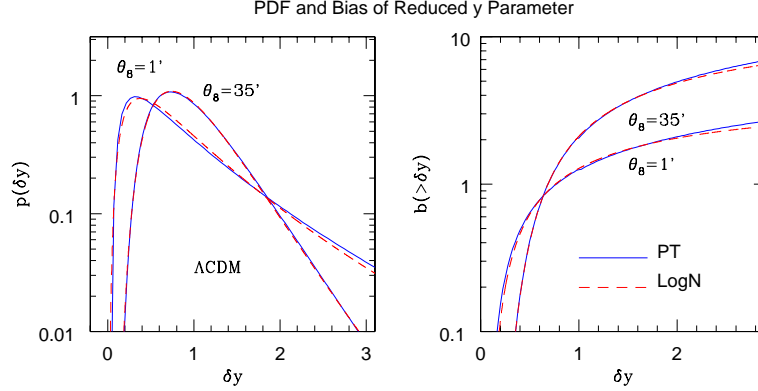


Figure 6. The PDF (left panel) and bias function (right panel) $b(> \delta y / \langle y \rangle)$ are plotted as a function of $\delta y / \langle y \rangle$. They are computed using two different approaches. The dashed lines show the analytical predictions from the hierarchical ansatz and the solid lines show the predictions from the lognormal distribution. The lines correspond to different angular scales as depicted.

the limiting situation when $\hat{\Omega}_1 = \hat{\Omega}_2$ we can recover the corresponding cumulants. Extending the above results to arbitrary order we can write:

$$\langle \kappa_s^p(\hat{\Omega}_1) \delta y_s^q(\hat{\Omega}_2) \rangle_c = C_{pq}^\eta \hat{C}_{p+q} [[\mathcal{I}_{\theta_s}]_{\text{wl}}^{(p-1)} [[\mathcal{I}_{\theta_s}]_{\text{sz}}^{(q-1)} [\mathcal{I}_{\theta_{12}}]] = C_{pq}^{\kappa y} [\langle \kappa_s^2 \rangle_c^{(p-1)}] [\langle \delta y_s^2 \rangle_c^{(q-1)}] \langle \kappa_s(\hat{\Omega}_1) \delta y_s(\hat{\Omega}_2) \rangle_c. \quad (21)$$

This is a generalization of the usual definition of cumulant correlators for the case of two different fields in this particular case convergence κ and δy_s . The smoothing angular scales and the window function are left completely arbitrary. These definitions can be also used to define mixed normalised one-point $S_N^{\kappa y}$ parameters (with $N = p + q$) involving two different fields by considering the limiting situation $\hat{\Omega}_1 = \hat{\Omega}_2$.

$$\hat{C}_{p+q} [[\mathcal{I}_{\theta_s}]^{p-1} \mathcal{I}_{\theta_{12}}] = \int_0^{r_s} \frac{\omega_{\text{wl}}^p(r) \omega_{\text{sz}}^q(r) b_\pi^q(r)}{d_A^{2(p+q-1)}(r)} [\mathcal{I}_{\theta_s}]_{\text{wl}}^{(p-1)} [\mathcal{I}_{\theta_s}]_{\text{sz}}^{(q-1)} [\mathcal{I}_{\theta_{12}}] dr; \quad [\mathcal{I}_{\theta_s}]_{\text{wl}} = \int \frac{d^2 \mathbf{l}}{(2\pi)^2} P_\delta \left(\frac{l}{d_A(r)} \right) W_{\text{TH}}^2(l\theta_s); \quad (22)$$

$$[\mathcal{I}_{\theta_s}]_{\text{sz}} = \int \frac{d^2 \mathbf{l}}{(2\pi)^2} P_\delta \left(\frac{l}{d_A(r)} \right) b_l^2(\theta'_s); \quad [\mathcal{I}_{\theta_{12}}] \equiv \int \frac{d^2 \mathbf{l}}{(2\pi)^2} P_\delta \left(\frac{l}{d_A(r)} \right) W_{\text{TH}}(l\theta_s) b_l(\theta'_s) \exp(\mathbf{l} \cdot \theta_{12}). \quad (23)$$

Though results can be derived for different smoothing angular scales, for simplicity we will only consider identical smoothing beam size $\theta_s = \theta'_s$. The hierarchical expression for the lowest order cumulant i.e. S_3^κ for convergence was derived by Hui (1998). He showed that his result agrees well with numerical ray tracing experiments. Later studies have shown that higher order cumulants and even the two-point statistics such as cumulant correlators can also be reliably modelled in a similar way (Munshi & Coles 1999; Munshi & Jain 1999a). More recently it was shown (Munshi et al. 2011a) that the statistics of tSZ too can be modelled according to the same prescription. In particular it was shown that the lognormal distribution can be used to predict the PDF and bias associated with the tSZ maps. We extend these results to the case of joint analysis of weak lensing and tSZ maps.

We will develop these results further to construct the full joint 2PDF simply using the individual bias functions for tSZ and weak lensing. The hierarchical ansatz allows us to write the joint 2PDF as:

$$p_{\kappa y}^{(i)}(\kappa_s^{(i)}, y_s) d\kappa_s^{(i)} dy_s = p_\kappa^{(i)}(\kappa_s^{(i)}) p_y(y_s) (1 + b_\kappa^{(i)}(\kappa_s) \xi_{12}^{\kappa y}(\theta_{12}) b_y(y_s)) d\kappa_s^{(i)} dy_s, \quad (24)$$

and its relation to the bias associated with collapsed objects in underlying density field $\eta = 1 + \delta$.

As an aside, it is simple to check that if we are dealing with tomographic redshift slices $\kappa_s^{(i)}$ and $\kappa_s^{(j)}$ of the same or different weak lensing surveys the corresponding cumulant correlators are defined as:

$$\hat{C}_{p+q}^{ij} [[\mathcal{I}_{\theta_s}]_{\text{wl}}^{p-1} [\mathcal{I}_{\theta_s}]_{\text{sz}}^{q-1} [\mathcal{I}_{\theta_{12}}]] = \int_0^{r_s} \frac{\omega_{(i)}^p(r) \omega_{(j)}^q(r) b_\pi^q(r)}{d_A^{2(p+q-1)}(r)} [\mathcal{I}_{\theta_s}]_{\text{wl}}^{(p-1)} [\mathcal{I}_{\theta_s}]_{\text{sz}}^{(q-1)} [\mathcal{I}_{\theta_{12}}] dr. \quad (25)$$

The expressions for the cumulant correlators are constructed by replacing $y_s(\hat{\Omega})$ in Eq. (21) with $\kappa_s^{(j)}(\hat{\Omega})$:

$$\langle \kappa_{(i)}^p(\hat{\Omega}_1) \kappa_{(j)}^q(\hat{\Omega}_2) \rangle_c = C_{pq}^\eta \hat{C}_{p+q} [[\mathcal{I}_{\theta_s}]^{p+q-2} [\mathcal{I}_{\theta_{12}}]] = C_{pq}^{\kappa y} \langle \kappa_{(i)}^2 \rangle_c^{(p-1)} \langle \kappa_{(j)}^2 \rangle_c^{(q-1)} \langle \kappa_s^{(i)}(\hat{\Omega}_1) \kappa_s^{(j)}(\hat{\Omega}_2) \rangle_c. \quad (26)$$

These expressions are quoted here for the highly nonlinear regime. As is well known a similar hierarchy develops in the quasilinear regime so the same analytical tools are applicable in such a situation. We will next use these expressions to compute the lower order moment of one and two-point PDFs.

The corresponding results for the Ostriker-Vishniac effect (and kinetic Sunyaev-Zel'dovich (kSZ) effect; Castro (2003)) will be presented elsewhere.

4 JOINT PROBABILITY DISTRIBUTION FUNCTION FOR κ_S AND \mathcal{Y}_S

To compute the bias associated with peaks in the convergence field we have to first develop an analytic expression for the generating function $\beta_{\kappa y}(z_1, z_2)$ for the convergence field κ_s and the tSZ field $\delta y_s = y_s - \langle y_s \rangle$. For that we will use the usual definition for the mixed two-point cumulant correlator $C_{pq}^{\kappa y}$:

$$C_{pq}^{\kappa y} = \frac{\langle \kappa_s^p(\hat{\Omega}_1) \delta y_s^q(\hat{\Omega}_2) \rangle_c}{\langle \kappa_s^2 \rangle_c^{p-1} \langle \delta y_s^2 \rangle_c^{q-1} \langle \kappa_s(\hat{\Omega}_1) \delta y_s(\hat{\Omega}_2) \rangle_c}. \quad (27)$$

(for a more detailed description of cumulant correlators see Munshi & Coles, 1999b). We will show that, like its density field counterpart, the two-point generating function for the convergence field κ_s can also be expressed (under certain simplifying assumptions) as a product of two generating functions $\beta(z)$ which can then be directly related to the bias associated with “hot-spots” in the convergence field. It is clear that the factorization of generating function actually depends on the factorization property of the cumulant correlators i.e. $C_{pq}^{\eta \eta'} = C_{p1}^\eta C_{q1}^{\eta'}$. Note that such a factorization is possible when the correlation of two patches in the directions $\hat{\Omega}_1$ and $\hat{\Omega}_2$ $\langle \kappa_s(\hat{\Omega}_1) \delta y_s(\hat{\Omega}_2) \rangle_c$ is smaller compared to the variance $\langle y_s^2 \rangle$ for the smoothed patches:

$$\beta_{\kappa y}(z_1, z_2) = \sum_{p,q} \frac{C_{pq}^{\kappa y}}{p!q!} z_1^p z_2^q = \sum_{p,q} \frac{1}{p!q!} \frac{z_1^p z_2^q}{\langle \kappa_s^2 \rangle_c^{p-1} \langle \delta y_s^2 \rangle_c^{q-1}} \frac{\langle \kappa_s^p(\hat{\Omega}_1) \delta y_s^q(\hat{\Omega}_2) \rangle_c}{\langle \kappa_s(\hat{\Omega}_1) \delta y_s(\hat{\Omega}_2) \rangle_c}. \quad (28)$$

Here z_1 and z_2 are dummy variables. We will now use the integral expression for cumulant correlators (Munshi & Coles 1999a) to express the generating function which in turn uses the hierarchical *ansatz* and the far field approximation as explained above:

$$\beta_{\kappa y}(z_1, z_2) = \sum_{p,q} \frac{C_{pq}^{\kappa y}}{p!q!} \frac{z_1^p}{\langle \kappa_s^2 \rangle_c^{p-1}} \frac{z_2^q}{\langle \delta y_s^2 \rangle_c^{q-1}} \frac{1}{\xi_{y\kappa}^{12}} \int_0^{r_s} dr d_A^2(r) \frac{\omega_{w1}^p(r) \omega_{\kappa}^q(r)}{d_A(r)^{2p} d_A(r)^{2q}} [\mathcal{I}_{\theta_s}]_{w1}^{p-1} [\mathcal{I}_{\theta_s}]_{sz}^{q-1} \mathcal{I}_{\theta_{12}}. \quad (29)$$

It is possible to further simplify the above expression by separating the summation over dummy variables z_1 and z_2 , which will be useful to establish the factorization property of two-point generating function for bias $\beta_{\kappa y}(z_1, z_2)$. We can now decompose the double sum over the two indices into two separate sums over individual indices. We do not use any of these specific models for clustering and only assume the hierarchal nature of the higher order correlation functions. In the past, primarily data from galaxy surveys have been analysed extensively using these *ansatze*. The motivation here is to show that cross-correlation statistics of weak-lensing surveys against the tSZ surveys can also be analysed using such techniques. The most general result for the lower order cumulant correlators in the large separation limit can be expressed as:

$$\beta_{\kappa y}(z_1, z_2) = \int_0^{r_H} dr d_A^2(r) \frac{\mathcal{I}_{\theta_{12}} \langle \kappa_s^2 \rangle_c}{\xi_{12}^{12} [\mathcal{I}_{\theta_s}]_{w1}} \beta_\eta \left(\frac{z_1}{\langle \kappa_s^2 \rangle_c} \frac{\omega_{w1}(r)}{d_A^2(r)} [\mathcal{I}_{\theta_s}]_{w1} \right) \frac{\langle \delta y_s^2 \rangle_c}{[\mathcal{I}_{\theta_s}]_{sz}} \beta_{\eta'} \left(\frac{z_2}{\langle \delta y_s^2 \rangle_c} \frac{\omega_{SZ}(r) b_\pi(r)}{d_A^2(r)} [\mathcal{I}_{\theta_s}]_{sz} \right). \quad (30)$$

The above expression is quite general and depends only on the small angle approximation (Limber 1954) and the large separation approximation and is valid for any given specific model for the generating function $\mathcal{G}_\delta(\tau)$. However, it is easy to notice that the projection effects as encoded in the line of sight integration do not allow us to write down the two-point generating function $\beta_{\kappa y}(z_1, z_2)$ simply as a product of two one-point generating functions $\beta_\kappa(z_1)$ and $\beta_y(z_2)$, as generally is the case for the density field $\eta = 1 + \delta$.

As in the case of the derivation of the probability distribution function for the smoothed convergence field κ_s , it will be much easier if we define a reduced smoothed convergence field η_s . The statistical properties of η_s are very similar to that of the underlying 3D density field (under certain simplifying approximation) and are roughly independent of the background geometry and dynamics of the universe. In a similar manner we also define the reduced y_s field η'_s . We define the reduced convergence η_s and the reduced tSZ y map η'_s respectively by the following expressions: $\eta_s = (\kappa_s - \kappa_m)/(-\kappa_m) = (1 + \kappa_s/|\kappa_m|)$ and $\eta'_s = \delta y_s / \langle y_s \rangle$. Where the minimum value of κ_m is defined as: $k_m = -\int_0^{r_s} dr \omega_{w1}(r)$ and $\langle y \rangle$ is the average value of the y parameter. It is easy to notice that the minimum value of the convergence field will occur in those lines of sight which are completely devoid of any matter, i.e. $\delta = -1$ all along the line of sight. We will also find out later that the cosmological dependence of the statistics of the κ_s field is encoded in k_m and this choice of the new variable η_s makes its related statistics almost independent of the background cosmology. Repeating the above analysis again for the η_s field, we can express the cumulant correlator generating function for the reduced convergence field η_s as:

$$\beta_{\eta \eta'}(z_1, z_2) = \int_0^{r_H} dr \frac{1}{|\kappa_m|} \frac{1}{\langle y_s \rangle} d_A^2(r) \frac{\mathcal{I}_{\theta_{12}} \langle \kappa_s^2 \rangle_c}{\xi_{12}^{12} [\mathcal{I}_{\theta_s}]_{w1}} \beta_\eta \left(|\kappa_m| \frac{z_1}{\langle \kappa_s^2 \rangle_c} \frac{\omega_{w1}(r)}{d_A^2(r)} [\mathcal{I}_{\theta_s}]_{w1} \right) \frac{\langle \delta y_s^2 \rangle_c}{[\mathcal{I}_{\theta_s}]_{sz}} \beta_{\eta'} \left(\langle y_s \rangle \frac{z_2}{\langle \delta y_s^2 \rangle_c} \frac{\omega_{SZ}(r) b_\pi(r)}{d_A^2(r)} [\mathcal{I}_{\theta_s}]_{sz} \right). \quad (31)$$

While the above expression is indeed very accurate and relates the generating function of the density field with that of the convergence field, it is difficult to handle for any realistic practical applications. Also it is important to notice that the scaling functions such as $h(x)$ for the density probability distribution function and $b(x)$ for the bias associated with over-dense objects (with $x = (1 + \delta)/\bar{\xi}_2^\delta$) are typically estimated from numerical simulations especially in the highly non-linear regime ($\bar{\xi}_2^\delta$ is the volume average of two-point correlation function). Such estimations are plagued by several uncertainties, such as the finite size of the simulation box. It was noted in earlier studies that such uncertainties lead to only a rather approximate estimation of $h(x)$. The estimation of the scaling function associated with the bias i.e. $b(x)$ is even more complicated due to the fact that the two-point quantities such as the cumulant correlators and the bias are more affected by the finite size of the catalogs. So it is not

fruitful to actually integrate the exact integral expression we have derived above and we will replace all line of sight integrals with its approximate values. The previous study by Munshi & Jain (1999) have used an exactly similar approximation to simplify the one-point probability distribution function for κ_s and found good agreement with ray tracing simulations. We will show that our approximation reproduces the numerical results quite accurately for a wide range of smoothing angle,

$$|\kappa_m| \approx \frac{1}{2} r_s \omega_{w1}(r_c); \quad \langle y \rangle \approx \frac{1}{2} r_s \omega_{SZ}(r_c) b_\pi(r_c); \quad 0 < r_c < r_s; \quad (32)$$

$$\langle \kappa_s^2 \rangle_c \approx \frac{1}{2} r_s \frac{\omega_{w1}^2(r_c)}{d_A^2(r_c)} \left[\int \frac{d^2 l}{(2\pi)^2} P_\delta\left(\frac{l}{d_A(r_c)}\right) W_{TH}^2(l\theta_s) \right]; \quad \langle \delta y_s^2 \rangle_c \approx \frac{1}{2} r_s \frac{b_\pi^2(r_c) \omega_{SZ}^2(r_c)}{d_A^2(r_c)} \left[\int \frac{d^2 l}{(2\pi)^2} P_\delta\left(\frac{l}{d_A(r_c)}\right) b_l^2(\theta_s) \right]; \quad (33)$$

$$\langle \kappa_s(\hat{\Omega}_1) \delta y_s(\hat{\Omega}_2) \rangle_c \approx \frac{1}{2} r_s \frac{\omega_{SZ}(r_c) \omega_{w1}(r_c)}{d_A^2(r_c)} \left[\int \frac{d^2 l}{(2\pi)^2} P_\delta\left(\frac{l}{d_A(r_c)}\right) W_{TH}(l\theta_s) b_l(\theta_s) \exp[i\mathbf{l} \cdot \theta_{12}] \right]. \quad (34)$$

Use of these approximations gives us the leading order contributions to these integrals and we can check that to this order we recover the factorization property of the generating function i.e. $\beta_{\eta\eta'}(z_1, z_2) = \beta_\eta(z_1) \beta_{\eta'}(z_2)$,

$$\beta_{\eta\eta'}(z_1, z_2) = \beta_\eta(z_1) \beta_{\eta'}(z_2) = \beta_{1+\delta}(z_1) \beta_{1+\delta'}(z_2) \equiv \tau(z_1) \tau(z_2). \quad (35)$$

So it is clear that at this level of approximation, due to the factorization property of the cumulant correlators, the bias function $b_\eta(x)$ associated with the peaks in the convergence field κ_s , beyond certain threshold, obeys a similar factorization property too, which is exactly the same as its density field counterpart. Earlier studies have established such a correspondence between the convergence field and the density field in the case of the one-point probability distribution function $p(\delta)$ (Munshi & Jain 1999b),

$$b_\eta(x_1) h_\eta(x_1) b_{\eta'}(x_2) h_{\eta'}(x_2) = b_{1+\delta}(x_1) h_{1+\delta}(x_1) b_{1+\delta'}(x_2) h_{1+\delta'}(x_2). \quad (36)$$

The following relation between $\beta_\eta(z)$ and $b_\eta(x)$ is useful for modelling. However, for all practical purpose we find that the differential bias $\beta_{>\eta}(y)$ as defined is simpler to measure from numerical simulations due to its cumulative nature:

$$b_\eta(x) h_\eta(x) = -\frac{1}{2\pi i} \int_{-i\infty}^{i\infty} dz \tau(z) \exp(xz); \quad b_\eta(>x) h_\eta(>x) = -\frac{1}{2\pi i} \int_{-i\infty}^{i\infty} dz \frac{\tau(z)}{z} \exp(xz). \quad (37)$$

Notice that the function $\tau(z)$ defined as $\tau(z) = \sum_p z^p C_{p1}/p!$ also acts as a generator for the C_{p1} parameters. The entire hierarchy of the C_{pq} can be constructed from the C_{p1} parameters i.e. $C_{pq} = C_{p1} C_{q1}$ at large separation limit. Using these results we can finally write down:

$$p_{\eta\eta'}(\eta, \eta') d\eta d\eta' = p_\eta(\eta) p_{\eta'}(\eta') (1 + b_\eta(\eta) \xi_{12}^{\eta\eta'} b_{\eta'}(\eta')) d\eta d\eta'; \quad \eta = \kappa_s/|\kappa_m|; \quad \eta' = \delta y_s/\langle y_s \rangle; \quad \xi_{12}^{\eta\eta'} = \langle \eta(\hat{\Omega}_1) \eta'(\hat{\Omega}_2) \rangle. \quad (38)$$

It is important to notice that although the bias $b_\eta(x)$ associated with the reduced convergence field and the underlying density field are exactly same, the variance associated with the density field is very high but the projection effects in the convergence field bring down the variance in the convergence field to less than unity which indicates that we have to use the integral definition of bias to recover it from its generating function (see Appendix A for more details). Finally, writing down the joint probability distribution function $p_{\kappa y}(\kappa_s, y_s)$ for the smoothed projected convergence field κ_s and the y_s in terms of their reduced versions η and η' :

$$p_{\kappa y}(\kappa_s, y_s) d\kappa dy = p_\kappa(\kappa_s) p_y(y_s) (1 + b_\kappa(\kappa_s) \xi_{12}^{\kappa y} b_y(y_s)) d\kappa dy; \quad b_y(y_s) = b_\eta(y_s/\langle y_s \rangle)/\langle y_s \rangle; \quad b_\kappa(\kappa_s) = b_\eta(\kappa_s/|\kappa_m|)/|\kappa_m|; \quad \xi_{12}^{\kappa y} \equiv \langle \kappa(\hat{\Omega}_1) y_s(\hat{\Omega}_2) \rangle = \xi_{12}^{\eta\eta'}/(|\kappa_m| \langle y_s \rangle). \quad (39)$$

In an earlier study, Munshi et al. (1999b) used similar arguments for the convergence maps to show that $p_\kappa(\kappa_s) = p_\eta(\kappa_s/|\kappa_m|)/|\kappa_m|$ and recently it was generalised by (Munshi et al. 2011) for the y -maps to $p_y(y_s) = p_\eta(y_s/\langle y_s \rangle)/\langle y_s \rangle$. If we notice that $\xi_{12}^{\kappa y} = \xi_{12}^{\eta\eta'}/(|\kappa_m| \langle y_s \rangle)$; then the above expressions helps us to write $b_\kappa(\kappa_s) = b_\eta(\kappa_s/|\kappa_m|)/|\kappa_m|$ and $b_y(y_s) = b_\eta(y_s/\langle y_s \rangle)/\langle y_s \rangle$. This is one of the main result of our analysis.

A similar result can of course be derived for cross-correlation of tSZ y_s map and weak lensing convergence maps $\kappa_s^{(i)}$ from individual tomographic bins. The joint PDF $p^{(i)}(\kappa_s^{(i)}, y_s)$ for tomographic maps $\kappa_s^{(i)}$ and projected y_s maps can be expressed in terms of the individual PDF $p^{(i)}(\kappa_s)$, $p(y_s)$ maps and the bias $b_\kappa^{(i)}(\kappa_s)$ and $b_y(y_s)$:

$$p^{(i)}(\kappa_s^{(i)}, y_s) d\kappa_s^{(i)} dy_s = p^{(i)}(\kappa_s) p(y_s) (1 + b_\kappa^{(i)}(\kappa_s^{(i)}) \xi_{12}^{(i)} b_y(y_s)) d\kappa_s^{(i)} dy_s; \quad b_\kappa^{(i)}(\kappa_s) = b_\eta(\eta)/|\kappa_m^{(i)}|; \quad b_y(y_s) = b_\eta(\eta')/\langle y_s \rangle; \quad \xi_{12}^{(i)} \equiv \xi_{12}^{\eta\eta'}/(|\kappa_m^{(i)}| \langle y_s \rangle). \quad (40)$$

Notice that the bias and one point PDF for both the projected convergence maps κ_s and tomographic maps $\kappa_s^{(i)}$ as well as for the tSZ map y are all constructed from the same underlying PDF p_η and the bias b_η associated with the 3D density distribution. The individual PDF $p_\kappa(\kappa_s)$ and $p_y(y_s)$ and the bias $b_\kappa(\kappa_s)$ and $b_y(y_s)$ have already been tested against numerical simulations and were found to be remarkably successful.

This technique will also allow for the computing of joint PDF of convergence maps for CMB lensing and the tSZ y_s maps. This can be achieved by replacing the κ_m in Eq. (39) with corresponding κ_m for the last scattering surface (LSS), i.e. $\kappa_m = -\int_0^{r_{LSS}} dr w_{w1}(r)$ where the source distance r_s is now replaced by the comoving distance to the LSS r_{LSS} . This is especially relevant given the recent evidence for a CMB lensing signal with WMAP and ACT (Das et al. 2011; Smidt et al. 2011). The results for the cumulant correlators can be modified analogously.

Though the results Eq. (39) and Eq. (40) are derived using the hierarchical ansatz the final results are remarkably independent of details of any of the assumptions that were used in deriving them. This is an indication of their more generic validity. Indeed it has been shown that the PDF and the bias for the tSZ and weak lensing fields can be constructed from equivalent but other valid descriptions of PDF and bias of underlying 3D density contrast. The lognormal distribution for the underlying PDF and bias provide one such description. In Appendix-B we have provided a short description of the lognormal distribution. The lognormal model based PDF and bias for κ_s and y_s are given by:

$$p_\kappa(\kappa_s) = p_{\ln}(\kappa_s/|\kappa_m|)/|k_m|; \quad p_y(\delta y_s) = p_{\ln}(\delta y_s/\langle y_s \rangle)/\langle y_s \rangle; \quad b_\kappa(\kappa_s) = b_{\ln}(\kappa/|\kappa_m|)/|k_m|; \quad b_y(\delta y_s) = b_{\ln}(\delta y_s/\langle y_s \rangle)/\langle y_s \rangle. \quad (41)$$

The resulting PDF and bias matches with the ones from perturbative calculations for higher smoothing angular scales.

As mentioned earlier, the joint probability of $p_{\kappa y}(\kappa_s, y_s)$ is a noisy statistics. The integrated measure or cumulative PDF of the convergence crossing a threshold κ_s and the tSZ field y_s crossing a threshold κ_0 and y_0 respectively is given by:

$$p_{\kappa y}(> \kappa_0, > y_0) = \int_{\kappa_0}^{\infty} d\kappa_s \int_{y_0}^{\infty} dy p_{\kappa y}(\kappa_s, y_s); \quad p_\kappa(> \kappa_0) = \int_{\kappa_0}^{\infty} d\kappa_s p_\kappa(\kappa_s); \quad p_y(> y_0) = \int_{y_0}^{\infty} dy_s p(y_s); \quad (42)$$

$$b_\kappa(> \kappa_0) = \int_{\kappa_0}^{\infty} d\kappa_s p(\kappa_s) b_\kappa(\kappa_s) / \int_{\kappa_0}^{\infty} d\kappa_s p(\kappa_s); \quad b_y(> y_0) = \int_{y_0}^{\infty} d\kappa_s p_y(y_s) b_y(y_s) / \int_{y_0}^{\infty} dy_s p_y(y_s). \quad (43)$$

The bias $b(> \kappa_0)$ is plotted in figure (5) for different redshift bins. As is clear the high κ regions in deeper redshift bins are more biased compared to the lower redshift bins. The bias is higher for larger smoothing angular scales. The figure (6) shows corresponding plots for the tSZ surveys.

The following statistics can be constructed from the cumulative bias to probe the joint SZ and weak-lensing cross-correlation to all orders:

$$\mathcal{B}(> \kappa_0, > y_0) = [b_\kappa(> \kappa_0) b_y(> y_0)]^{1/2} = \frac{1}{\sqrt{\xi_{12}^{\kappa y}}} \left[\frac{p_{\kappa y}(> \kappa_0, > y_0)}{p_\kappa(> \kappa_0) p_y(> y_0)} - 1 \right]^{1/2} \quad (44)$$

It is important to notice that our modelling of the PDF p_κ and p_y is independent of the modelling of respective variances. The variance calculations for y_s depend on inputs such as the detailed modelling of bias and its redshift evolution that can be independently checked by comparing with simulations. However, given a correct variance the lognormal model or the hierarchical ansatz can be used to model the entire PDF as we have shown. For construction of the PDF of the scaled or reduced tSZ i.e. η we also need the average $\langle y_s \rangle$. The modelling of average $\langle y_s \rangle$ is independent of the construction of PDF. However what we have shown here is that given these two inputs we can reliably predict the PDF of y . While the PDF of reduced tSZ field η is independent of cosmology the dependence of y parameter is encoded in the definition of reduced y_s field $\eta' = \delta y_s / \langle y_s \rangle$. The convergence PDF is defined in terms of the PDF for the reduced convergence $\eta = \kappa_s / |\kappa_m|$. The PDF for the reduced convergence κ_s as well as the scaled tSZ map y_s are both shown to be same as the PDF of underlying ark matter distribution δ . The dependence of p_κ on cosmological parameters is encoded in the definition of κ_m . The cosmological parameter dependence of bias $b_\kappa(\kappa_s)$ and $b_y(y_s)$ is encoded in $\langle y_s \rangle$ and κ_m .

It is also interesting that our calculations show that the PDF of *projected* or 2D convergence as well as the tSZ maps are described by the underlying 3D density contrast δ which is in agreement with (Munshi & Jain 2000, 2001) and provides robust mathematical justification for the use of lognormal model and its link to linear biasing prescription.

A simple order of magnitude estimate for the weak lensing cumulants is $S_p^\kappa = \langle \kappa_s^p \rangle / \langle \kappa_s^2 \rangle^{p-1}$ is given by $S_p^\kappa = S_p / |\kappa_m|^{p-2}$. The cumulants of the field $\delta y_s / \langle y_s \rangle$ simply follows that of the underlying density contrast. The normalised cumulant correlators of the smoothed convergence field κ_s and the field $\delta y_s / \langle y_s \rangle$ is given by $C_{pq}^{\kappa y} = C_{pq}^{\eta \eta'} / |\kappa_m|^{p-1}$.

5 INCLUSION OF NOISE

In our discussion so far, we have ignored the effect of noise in the estimation of one- and two-point PDFs. If we assume the noise n to be uncorrelated with the signal, the noisy one-point PDFs can be expressed as a convolution of the signal and noise PDF:

$$p_n^{(i)}(\kappa_s) = \int_{-\infty}^{\infty} p_{\kappa_s}^{(i)}(\kappa_s - n) g_\kappa^{(i)}(n) dn; \quad p_n(y_s) = \int_{-\infty}^{\infty} p_y(y_s - n) g_y(n) dn. \quad (45)$$

We have denoted the i -th tomographic noisy convergence PDF by $p_n^{(i)}(\kappa)$. The noisy y -PDF is denoted by $p_n(y)$. The noise in y -map is due the detector noise and in κ maps due to intrinsic ellipticity distribution of galaxies. The noise PDF in each case is often assumed to be Gaussian; we will use $g_\kappa^{(i)}(n)$ and $g_y(n)$ to denote the PDFs of the noise in y -map and tomographic κ maps respectively. The modification of the joint PDF of κ_s and y_s due to noise can be computed using a similar convolution:

$$p_n^{(i)}(\kappa_s, y_s) = \int_{-\infty}^{\infty} p^{(i)}(\kappa_s - n_1, y_s - n_2) g_\kappa^{(i)}(n_1) g_y(n_2) dn_1 dn_2 \quad (46)$$

Using Eq. (39) with Eq. (46), we derive the following expression:

$$n_\kappa^{(i)}(\kappa_s, y_s) = p_n^{(i)}(\kappa_s) p_n(y_s) (1 + b_n^{(i)}(\kappa_s) \xi_{12}^{\kappa y} b_n(y_s)). \quad (47)$$

The inclusion of noise thus preserves the factorization of the 2PDF which can be expressed in terms of noisy PDFs and bias functions. The presence of noise does not affect the two-point correlation function $\xi_{12}^{\kappa y}$; The noisy bias functions $b_n^{(i)}(\kappa)$ and $b_n(y)$ for κ and y are respectively defined by the following expressions:

$$b_n^{(i)}(\kappa) = \int_{-\infty}^{\infty} p_{\kappa_s}^{(i)}(\kappa_s - n) b_{\kappa_s}^{(i)}(\kappa_s - n) g_{\kappa}(n) dn / \int_{-\infty}^{\infty} p_{\kappa}^{(i)}(\kappa_s - n) g_{\kappa}^{(i)}(n) dn \quad (48)$$

$$b_n^{(i)}(> \kappa_s) = \int_{\kappa}^{\infty} p_n^{(i)}(\kappa_s) b_n^{(i)}(\kappa_s)(\kappa)_s d\kappa_s / \int_{\kappa}^{\infty} p_n^{(i)}(\kappa) d\kappa; \quad (49)$$

We have defined a cumulative bias function $b_n^{(i)}(> \kappa)$ for the noisy map. It is constructed from the bias $b_n^{(i)}(\kappa)$ and the one-point PDF $p_n^{(i)}(\kappa)$ in an exactly similar way as the noisefree PDF and bias function Eq. (43). The noise in convergence maps depends on the intrinsic ellipticity distribution of galaxies σ_e . For a smoothing radius θ_s the noise variance σ_{κ} that completely determines the noise PDF $g_{\kappa}^{(i)}(n_1)$ is given by: $\sigma_{\kappa} = \sigma_e^2 / 2\pi n_g \theta_s^2$. Here n_g is the number density of galaxies per arcmin². Similar expressions can be used to define the $b_n^y(> y)$:

$$b_n(y_s) = \int_{-\infty}^{\infty} p_y(y_s - n) b_y(y_s - n) g_{y_s}(n) dn / \int_{-\infty}^{\infty} p_{\kappa}^{(i)}(\kappa_s - n) g_{\kappa}^{(i)}(n) dn \quad (50)$$

$$b_n(> y_s) = \int_{y_s}^{\infty} p_n^{(i)}(y_s) b_n^{(i)}(y_s) dy_s / \int_{y_s}^{\infty} p_n(y_s) dy_s. \quad (51)$$

These expressions are sufficient to compute the cumulative bias for weak lensing tomographic slices and y-maps; these bias functions are enough to construct the entire family of two-point cumulant correlators involving weak lensing and tSZ maps even in the presence of noise.

6 CONCLUSION

We have presented a detailed analysis of the higher-order (non-Gaussian) cross-correlation of tSZ maps and the projected as well as redshift-resolved tomographic maps from weak lensing surveys.

What distinguishes our work in this paper is that it extends earlier studies which have focused mainly on cross-correlation analysis at the level of power spectrum. The tSZ maps as well as the maps derived from weak lensing surveys are intrinsically non-Gaussian even at large angular scales. In this study we extend the cross-correlation statistics to higher-order. We employ the mixed cumulants and their correlators that can extract higher-order statistics that are useful in probing the thermal history of the Universe when studied in association with redshift resolved tomographic weak lensing data. The statistics that we introduce can be used in projection (2D) or with tomographic information, independent of any analytical modelling to analyze simulations or observational data. The estimators presented here are generic and can be used for other cross-correlation studies involving two different *arbitrary* fields. The mixed cumulants and their correlators defined in this paper are the lower order moments of the corresponding one-point or two-point PDFs and associated bias. These statistics generalize cumulant correlators defined in (Munshi 2000) for weak lensing surveys and in (Munshi et al. 2011a,b) for tSZ datasets, and are useful in cross-correlating these two independent data sets.

Beyond the order-by-order calculation, a generic prediction for the cumulants or their correlators to an arbitrary order is required. This can be achieved by adopting the generating function formalism inherent in models based on the *hierarchical ansatz*. We have employed a generic version of the hierarchical ansatz as well as the lognormal distribution to model the underlying mass distribution. Both of these have been studied extensively in the literature. These particular models go beyond the lowest order in correlation hierarchy. For the hierarchical model, the generating function is parametrized in terms of a single parameter ω which is fixed using inputs from numerical simulations, and is the only freedom allowed in this model. In the perturbative regime this parameter can be calculated analytically. Indeed, modelling of pressure fluctuations in terms of the underlying density distribution is more complicated, and we rely on a redshift dependent linear biasing model that is expected to be valid at large angular scales (Munshi et al. 2011a,b). More complicated models can be considered in this framework using additional inputs from numerical simulations; here we have tried to keep the modelling as simple as possible. The halo model can be used for the construction of the lowest order cumulant correlators. However, in such an approach, results can be derived only in an order-by-order manner and the relevant PDF and bias needs to be constructed using suitably truncated Edgeworth expansions. As mentioned previously, the PDF and bias for the weak lensing data have been studied by many authors using both the hierarchical ansatz and the lognormal distribution. The studies have shown how accurately these distributions can model numerical simulations. In more recent studies, the hierarchical ansatz has also been used successfully in tSZ modelling. Based on this success, our primary goal in this study has been to extend such analysis to compute the joint PDF of κ_s and y_s along same or different lines of sight. In lieu of individual haloes, we consider here the diffuse tSZ component that correlates with the large-scale weak lensing shear and convergence.

We have shown that the two different variables, i.e. the scaled tSZ parameter $\eta' = \delta y_s / \langle y_s \rangle$ and the reduced convergence field $\eta = \kappa_s / \kappa_m$ can be introduced to simplify the analysis. Employing the hierarchical ansatz, we next show that the statistics of these reduced variables are the same as the underlying density $\rho/\rho_b = 1 + \delta$ under certain simplifying approximations, which is true both at the level of one and two-point statistics. Thus, the final results do not depend on the specific details of the input parameters of hierarchical ansatz, and may point to a wider applicability. The joint distribution involving κ_s and y_s can thereby be written in terms of $p(\eta)$ and $b(\eta)$ with suitable scaling involving $\langle y_s \rangle$ and

κ_m . The detailed construction of the PDF is insensitive to modelling of the bias of the hot ionized gas with respect to the dark matter distribution. The detailed prescription for such bias enters the results through the computation of the variance and the two-point correlation function $\xi_{y\kappa}(\theta_{12})$.

Specific models of hierarchical clustering have previously been employed to understand the tSZ effect (see e.g. (Valageas, Schaefer & Silk 2001; Valageas & Silk 1999; Valageas & Schaeffer 2000)). However, they have been employed to model contribution from the collapsed objects (e.g. massive clusters). In this case, the tail of the scaling functions $h(x)$ and $b(x)$ are relevant as they describe the collapsed objects. In addition to these inputs, the modelling would involve a prescription for the hydrodynamic equilibrium of the gas residing in the halo. These can be used to model the PDF of $y(\hat{\Omega})$, i.e. $p_y(y)$ or $b_y(y)$. The modelling considered here is complementary to our analysis. We have considered redshift dependent linear biasing to model the shock heated gas in the inter-galactic medium that produces a diffuse tSZ effect. The linear biasing model has been studied at the level of the power spectrum by many authors (Goldberg & Spergel 1999a,b; Peiris & Spergel 2000). The hierarchical model that we use here was also previously used by Zhang, Pen & Wang (2002), Cooray, Tegmark & Hu (2000) and (Cooray 2000, 2001) for modelling lower order moments where the linear biasing model for the pressure fluctuations was assumed. Our results are natural generalizations of such studies to higher order multi-spectra to study the non-Gaussian aspects of tSZ maps.

The generic statistics that we have developed for lower order cumulant and their correlators can be used to probe the higher order correlation functions in a model independent way. The redshift-resolved tomographic weak lensing maps when cross-correlated with tSZ maps can provide valuable information of the redshift evolution of the clustering of the ionized gas. The cumulant correlators are collapsed higher order correlation functions and typically carry more signal to noise than ordinary higher order correlation functions. Hence, they are useful for analyzing data from numerical simulations and observational maps. We have presented detailed analytical derivations regarding the inclusion of noise in our analysis that follow from simple convolution. It is important to realize that the modelling we have presented is highly constrained without much room for any additional fine-tuning. The bias that appears in the independent analysis of the tSZ maps (i.e. $b_y(y_s)$) and the bias that is required to model the statistics of weak lensing maps (i.e. $b_\kappa(\kappa_s)$) are enough to model the higher order cross-correlations between these two maps to an arbitrary order. This could provide a much needed consistency check for any possible cross-contamination, as well as inputs from “gastrophysics”. It is moreover interesting that the tail end of the same scaling functions $h(x)$ and $b(x)$ that we have adopted here are used to model the tSZ.

It is known that the IGM is most likely have been preheated by non-gravitational sources. The feedback from SN or AGN can play an important role. The analytical modelling of such non-gravitational processes is rather difficult. Numerical simulations (Springel et al 2001; da Silva et al. 2000, 2004; White, Hernquist & Springel 2002; Lin et al. 2004) have shown that the amplitude of the tSZ signal is sensitive to the non-gravitational processes, e.g. the amount of radiative cooling and energy feedback. It is also not straightforward to disentangle contributions from competing processes. The inputs from simulations are vital for any progress. Our analytical results should be treated as a first step in this direction. We have focused mainly on large angular scales where we expect the gravitational process to dominate and such effects to be minimal. Indeed, studies involving simulations have found that the cross-spectra involving tSZ and wl maps are less affected by the baryonic physics (Shao et al. 2011a).

Our results are derived using cross-correlating tomographic slices from weak lensing surveys and the projected tSZ surveys. With suitable modification, they can be equally applicable to cross-correlation studies using tomographic maps from the same or different weak lensing surveys. The results can also be used to study the weak lensing of CMB by cross-correlating it against tomographic weak lensing maps or tSZ maps. To move beyond a tomographic or projected survey, a complete 3D analysis can be invoked. An analysis similar to what has been presented here for the kinetic Sunyaev-Zel’dovich effect (e.g. Shao et al. (2011b)) can provide valuable information about the reionization history of the Universe (Munshi et al. 2011; in preparation).

7 ACKNOWLEDGEMENTS

DM and PC acknowledges support from STFC standard grant ST/G002231/1 at School of Physics and Astronomy at Cardiff University where this work was completed. SJ and JS acknowledge support from the US Department of Education through GAANN at UCI. We thank Alan Heavens for useful discussions. It is also a pleasure for us to thank Martin Kilbinger for related collaboration. We thank Francis Bernardeau for supplying a copy of his code which was used to compute the bias and the PDF from hierarchical ansatz.

REFERENCES

- Albrecht A. et al., 2011, arXiv:0901.0721
- Balian, R., Schaeffer, 1989, A&A, 220, 1
- Bernardeau F., Colombi S., Gaztanaga E., Scoccimarro R., 2002, Phys.Rept.,367, 1
- Bernardeau F., 1992, ApJ, 392, 1
- Bernardeau F., 1994, A&A, 291, 697
- Bernardeau F., 1998, A&A, 338, 375
- Bernardeau, F., Kofman, L. 1995, ApJ, 443, 479
- Bernardeau F., Schaeffer R., 1999, A&A, 349, 697
- Bernardeau F., Schaeffer R., 1992, A&A, 255, 1

- Birkinshaw M. 1999, Phys.Rep, 310, 98
- Bi H.G., Davidson A.F. 1997, ApJ, 479, 523
- Bouchet F.R. & Gispert R., 1999, New Astronomy, 4, 443
- Bouchet, F., Strauss, M. A., Davis, M., Fisher, K. B., Yahil, A., Huchra, J. P. 1993, ApJ, 417, 36
- Castro P.G., 2003, PRD, 67, 123001
- Cao L., Liu J. Fang L.-Z., 2007, ApJ, 661, 641
- Cen R., Ostriker J.P., 1999, ApJ, 514, 1
- Colombi, S., Bouchet, F. R., Hernquist, L., 1996, ApJ, 465, 14
- Colombi S., Bouchet F.R., Schaeffer R., ApJ. Suppl.,96,1996,401
- Colombi, S., Bernardeau, F., Bouchet, F. R., Hernquist, L. 1997, MNRAS, 287, 241
- Colombi S., 1994, ApJ, 435, L536
- Coles P., Jones B. 1991, MNRAS, 248,1
- Cooray A., Seth R., 2002, Phys. Rep. 372, 1
- Cooray, A., Hu, W., Astrophys. J., 2002, 574, 19
- Cooray A., Hu W. 2001, ApJ, 548, 7
- Cooray A., Hu W., 2000, ApJ, 535, L9
- Cooray A., Tegmark M., Hu W., 2000, ApJ, 540, 1
- Cooray A, 2000, PRD, 62, 103506
- Cooray A, 2001, PRD, 64, 063514
- Das S., et al., 2011, PRL, 107:021301
- Delabrouille J., Cardoso J., Patanchon G., 2003, MNRAS, 330, 807
- Dunkley J. et al., 2010, arXiv:1009.0866
- Fowler J. W. et al. 2010, ApJ, 722, 1148
- Fry J. N., 1984, ApJ, 279, 499
- Goldberg D.M., Spergel D.N., 1999, PRD, 59, 103001
- Goldberg D.M., Spergel D.N., 1999, PRD, 59, 103002
- Hamilton, A. J. S. 1985, ApJ, 292, L35
- Hansen F.K., Branchini E., Mazzotta P., Cabella P., Dolag K. MNRAS, 2005, 361, 753
- Hallman E.J., O'Shea B.W., Smith B.D., Norman M.L., Harkness R., Wagner R., 2007, ApJ, 671, 27
- Hallman E.J., O'Shea B.W., Smith B.D., Burns J.O., Norman M.L., 2009, ApJ, 698, 1759
- Hirata, C. M., Seljak, U., 2004, PRD, 70, 063526
- Hirata, C., Seljak, U., Phys. Rev. D, 2003, 68, 083002
- Hui L., 1999, ApJ, 519, L9
- Huterer, D., *et al.*, MNRAS, 2006, 366, 101
- Jones M. E. et al. 2005, MNRAS, 357, 518
- Joudaki S., Smidt J., Amblard A., Cooray A., 2010, JCAP, 1008, 027
- Joudaki S., Kaplinghat M., 2011, arXiv:1106.0299
- Kaiser N., 1998, ApJ, 498, 26
- Kayo I., Taruya A., Suto Y. 2001, ApJ, 561, 22
- Kofman L., Bertschinger E., Gelb J. M., Nusser A., Dekel A. 1994, ApJ, 420, 44
- Komatsu E., Seljak U. 2002, MNRAS, 336,1256
- LaRoque S.J., Bonamente M., Carlstorm J.E., Joy M.K., Nagai D., Reese E.D., Dawson K.S., 2006, ApJ, 652, 917
- Leach S.M., et al., 2008, A&A, 491, 597
- Lin K.-Y, Woo T.-P., Tseng Y.-H., Lin L., Chiueh T. 2004, ApJ, 608, L1
- Limber D.N., 1954, ApJ, 119, 665
- Lueker, M., et al 2010, ApJ, 719,1050
- Matarrese S., Lucchin F, Moscardini L, Saez D.,1992, MNRAS,259,437.
- Ma, Z., Hu, W., Huterer, D., Astrophys. J., 2005, 636, 21
- McDonald, P., Trac, H., Contaldi, C., MNRAS, 2006, 366, 547
- Munshi D., Coles P., Melott A.L., 1999a, MNRAS, 307, 387
- Munshi D., Coles P., Melott A.L., 1999b, MNRAS, 310, 892
- Munshi D., Melott A.L., Coles P., 1999c, MNRAS, 311, 149
- Munshi D., Valageas P., van Waerbeke L., Heavens A., 2008, PhR, 462, 67
- Munshi D., Jain B., 2000, MNRAS, 318, 109
- Munshi D., Jain B., 2001, MNRAS, 322, 107
- Munshi D., Valageas P., Barber A. J., 2004, MNRAS, 350, 77

- Munshi D., Valageas P., 2004, MNRAS, 354, 1146
- Munshi D., Kitching T., Heavens A., Coles P., 2010, MNRAS, (in press)
- Munshi D., Melott A. L., Coles P., 2000, MNRAS, 311, 149
- Munshi D., Heavens A. 2010, MNRAS, 401, 2406
- Munshi D., Heavens A., Cooray A., Valageas P. 2011, MNRAS, (in press)
- Munshi D., Sahni V., Starobinsky A., 1994, ApJ, 436, 517
- Munshi D., MNRAS, 2000, 318, 145
- Munshi D., Joudaki S., Smidt J., Coles P. 2011, MNRAS (submitted)
- Munshi D., Smidt J., Joudaki S., Coles P. 2011, MNRAS, (in press)
- Navarro J., Frenk C., White S.D.M 1996, ApJ, 462, 563
- Peiris H., Spergel D., 2000, ApJ, 540, 605
- Persi F., Spergel D. Cen R., Ostriker J., 1995, ApJ, 442, 1
- Peebles P.J.E., 1971, Physical cosmology, Princeton Series in Physics.
- Planck Collaboration, 2006, astro-ph/0604069
- Planck Collaboration, 2011, arXiv:1101.2024
- Press W., Sechter P., 1974, Astrophys.J, 187, 425
- Rauch M., 1998, Annual Review of A&A, 1, 267
- Rephaeli Y. 1995, ARA&A, 33, 541
- Reese E.D., Carlstorm J.E., Joy M., Mohr J.J., Grego L., Holzapfel W.L., 2002, ApJ, 581, 53
- Refregier A., Komatsu E., Spergel D.N., Pen U.-L., 2000, PRD, 61, 123001
- Roncarelli M., Moscardini L., Borgano S., Dolag K., 2007, MNRAS, 378, 1259
- Rosati P., Borgani S., Norman C., 2002, Annual Review of A&A, 40, 539
- Scoccimarro R., Colombi S., Fry J.N., Frieman J.A., Hivon E., Melott A., 1998, ApJ., 496, 586
- Seljak U., MNRAS, 2000, 318, 203
- Seljak U., Burwell J., Pen U.-L. 2001, Phys.Rev. D63, 063001
- Shao J., Zhang P., Lin W., Jing Y., 2011, ApJ, 730, 127
- Shao J., Zhang P., Lin W., Jing Y., Pan J., 2011, MNRAS, 413, 628
- da Silva et al., Barbosa A.C., Liddle A.R., Thomas P.A., 2000, MNRAS, 317, 37
- da Silva A.C., Kay S.T, Liddle A.R., Thomas P.A., 2004, MNRAS, 348, 1401
- Smidt J., Joudaki S., Serra P., Amblard A., Cooray A., 2010, PRD, 81, 123528
- Smidt J., Cooray A., Amblard A., Joudaki S., Munshi D., Santos M.G., Serra P., 2011, APJL, 728, 1, L1
- Smith R. E. et al., 2003, MNRAS, 341, 1311
- Springel V., White M. & Hernquist L., 2001, ApJ, 549, 681
- Sunyaev R.A., Zel'dovich Ya B., 1980, ARA&A, 18, 537
- Sunyaev R.A., Zel'dovich Ya B., Comments Astrophys. Space Phys, 4, 173
- Szapudi I., Szalay A.S., 1993, ApJ, 408, 43
- Szapudi I., Colombi S., 1996, ApJ, 470, 131
- Szapudi I., Szalay A.S., 1997, ApJL, 481, 1
- Takada M. Jain B., 2002, MNRAS, 337, 875
- Takada M. Jain B., 2003, MNRAS, 340, 580
- Taruya A., Takada M., Hamana T., Futamase T., 2002, ApJ, 571, 638
- Valageas P., 2000a, A&A, 354, 767
- Valageas P., 2000b, A&A, 356, 771
- Valageas P., 2002, A&A, 382, 412
- Valageas P., Schaeffer R., Silk J. 2001, A&A, 366, 363
- Valageas P., Silk J., 1999, A&A, 350, 725
- Valageas P., Schaeffer R., 2000, A&A, 359, 821
- White M., Hernquist V. & Springel V., 2002, ApJ, 579, 16
- White S.D.M, 1979, MNRAS, 186, 145
- White, M., Astropart. Phys., 2004, 22, 211
- Zhang P., Pen U.-Li., Wang B., 2002, ApJ, 577, 555
- Zhang P., Pen U.-Li., 2001, ApJ, 549, 18
- Zhang P., Pen U.-Li, Trac H., 2004, MNRAS, 355, 451
- Zhang P., Seth R.K., 2007, ApJ, 579, 16

APPENDIX A: GRAVITATIONAL CLUSTERING AND THE HIERARCHICAL ANSATZ

The lower order cumulants and cumulant correlators as well as the one- and two-point PDFs are commonly used statistics in cosmology to quantify clustering (Bernardeau et al 2002). Use of generating function techniques to go beyond order by order calculations is an important milestone in this direction (Peebles 1971; Balian & Schaeffer 1989; Bernardeau 1992; Bernardeau & Schaeffer 1992; Bernardeau 1994). This approach is complimentary to the halo model based approach that rely on Press-Sechter mass formalism (Press & Schechter 1974). We provide a very brief review of this formalism in this appendix.

A1 The Generating Function

In scaling analysis of the probability distribution function (PDF) the void probability distribution function (VPF), denoted as $P_v(0)$, plays most fundamental role, which can be related to the generating function of the cumulants or S_N parameters, $\phi(z)$ (White 1979; Balian & Schaeffer 1989):

$$P_v(0) = \exp(-\bar{N}\sigma(N_c)) = \exp\left(-\phi(N_c)/\bar{\xi}_2^\delta\right). \quad (\text{A1})$$

Where $P_v(0)$ is the probability of having no “particles” in a cell of volume v , \bar{N} is the average occupancy of these “particles” and $N_c = \bar{N}\bar{\xi}_2^\delta$ and $\sigma(z) = -\phi(z)/z$. Here $\phi(z) = \sum_{p=1}^{\infty} S_p/p! z^p$ is a generating function for S_N parameters. The generating function $\mathcal{G}(\tau)$ for the vertex amplitudes ν_p is related to $\phi(z)$. A more specific model for $\mathcal{G}(\tau)$ is generally used to make more specific predictions (Balian & Schaeffer 1989):

$$\mathcal{G}_\delta(\tau) = \left(1 + \tau/\kappa_a\right)^{-\kappa_a}. \quad (\text{A2})$$

The parameter κ_a is related to the parameter ω_a to be introduced later. The two generating functions are related by the following expression (Balian & Schaeffer 1989; Bernardeau & Schaeffer 1992, 1999):

$$\phi(z) = z\mathcal{G}_\delta(\tau) - \frac{1}{2}z\tau \frac{d}{d\tau}\mathcal{G}_\delta(\tau); \quad \tau = -z \frac{d}{d\tau}\mathcal{G}_\delta(\tau). \quad (\text{A3})$$

However a more detailed analysis is needed to include the effect of correlation between two or more correlated volume elements which will provide information about bias, cumulants and cumulant correlators (Bernardeau & Schaeffer 1992; Munshi, Coles & Melott 1999a,b; Munshi, Melott & Coles 1999c). Notice that $\tau(z)$ (also denoted by $\beta(z)$ in the literature) plays the role of generating function for factorized cumulant correlators $C_{p1}^{\eta\eta'}$ ($C_{pq} = C_{p1}^{\eta\eta'} C_{q1}^{\eta'\eta'}$): $\tau(z) = \sum_{p=1}^{\infty} C_{p1}^{\eta\eta}/p! z^p$.

A2 Generating Functions and the Construction of the PDF and Bias

The hierarchical form of higher order correlation functions appear in two completely different regimes in gravitational clustering. The generating function approach is a convenient technique to sum up to arbitrary information that leads to construction of entire probability distribution functions.

A2.1 The Highly Non-linear Regime

The PDF $p(\delta)$ and bias $b(\delta)$ can be related to their generating functions VPF $\phi(z)$ and $\tau(z)$ respectively by following equations (Balian & Schaeffer 1989; Bernardeau & Schaeffer 1992, 1999)

$$p(\delta) = \int_{-\infty}^{\infty} \frac{dz}{2\pi i} \exp\left[\frac{(1+\delta)z - \phi(z)}{\bar{\xi}_2}\right]; \quad b(\delta)p(\delta) = \int_{-\infty}^{\infty} \frac{dz}{2\pi i} \tau(z) \exp\left[\frac{(1+\delta)z - \phi(z)}{\bar{\xi}_2}\right]. \quad (\text{A4})$$

It is clear that the function $\phi(z)$ completely determines the behavior of the PDF $p(\delta)$ for all values of δ . However different asymptotic expressions of $\phi(z)$ govern the behavior of $p(\delta)$ for different intervals of δ . For large y we can express $\phi(z)$ as: $\phi(z) = az^{1-\omega}$. Here we have introduced a new parameter ω for the description of VPF. Typically initial power spectrum with spectral index $n = -2$ (which should model CDM like spectra we considered in our simulations at small length scales) produces a value of .3 which we will be using in our analysis (Colombi, Bouchet & Hernquist 1996; Colombi, Bouchet & Schaeffer 1996; Colombi et al. 1997). The VPF $\phi(z)$ and its two-point analog $\tau(z)$ both exhibit singularity for small but negative value of z_* ,

$$\phi(z) = \phi_* - a_*\Gamma(\omega_*)(z - z_*)^{-\omega_*}; \quad \tau(z) = \tau_* - b_*(z - z_*)^{-\omega_*-1}. \quad (\text{A5})$$

For the factorizable model of hierarchical clustering the parameter ω_* takes the value $-3/2$ and a_* and b_* can be expressed in terms of the nature of the generating function $\mathcal{G}_\delta(\tau)$ and its derivatives near the singularity τ_* (Bernardeau & Schaeffer 1992):

$$a_* = \frac{1}{\Gamma(-1/2)} \mathcal{G}'_\delta(\tau_*) \mathcal{G}''_\delta(\tau_*) \left[\frac{2\mathcal{G}'_\delta(\tau_*) \mathcal{G}''_\delta(\tau_*)}{\mathcal{G}'''_\delta(\tau_*)} \right]^{3/2}; \quad b_* = \left[\frac{2\mathcal{G}'_\delta(\tau_*) \mathcal{G}''_\delta(\tau_*)}{\mathcal{G}'''_\delta(\tau_*)} \right]^{1/2}. \quad (\text{A6})$$

As mentioned before the parameter k_a which we have introduced in the definition of $\mathcal{G}_\delta(\tau)$ can be related to the parameters a and ω appearing in the asymptotic expressions of $\phi(z)$ (Balian & Schaeffer 1989; Bernardeau & Schaeffer 1992)

$$\omega = k_a/(k_a + 2),; \quad a = \frac{k_a + 2}{2} k_a^{k_a/k_a + 2}. \quad (\text{A7})$$

Similarly the parameter z_s which describe the behavior of the function $\phi(z)$ near its singularity can be related to the behavior of $\mathcal{G}(\tau)$ near τ_s which is the solution of the equation (Balian & Schaeffer 1989; Bernardeau & Schaeffer 1992)

$$\tau_* = \mathcal{G}'_\delta(\tau_*)/\mathcal{G}''_\delta(\tau_*), \quad (\text{A8})$$

finally we can relate k_a to y_* by following expression (see Eq. (A7)):

$$z_* = -\frac{\tau_*}{\mathcal{G}'(\tau_*)}; \quad -\frac{1}{z_*} = x_* = \frac{1}{k_a} \frac{(k_a + 2)^{k_a + 2}}{(k_a + 1)^{k_a + 1}}. \quad (\text{A9})$$

The newly introduced variable x_* will be useful to define the large- δ tail of the PDF $p(\delta)$ and the bias $b(\delta)$. Different asymptotes in $\phi(z)$ are linked with behavior of $p(\delta)$ for various regimes of δ . For very large values of variance i.e. ξ_2 it is possible to define a scaling function $p(\delta) = h(x)/\xi_2^2$ which will encode the scaling behavior of PDF, where x plays the role of the scaling variable and is defined as $x = (1 + \delta)/\xi_2$. We list different ranges of δ and specify the behavior of $p(\delta)$ and $b(\delta)$ in these regimes (Balian & Schaeffer 1989)

$$(\bar{\xi}_2^\delta)^{-\omega/(1-\omega)} \ll 1 + \delta \ll \bar{\xi}_2^\delta; \quad p(\delta) = \frac{a}{(\bar{\xi}_2^\delta)^2} \frac{1-\omega}{\Gamma(\omega)} \left(\frac{1+\delta}{\bar{\xi}_2^\delta} \right)^{\omega-2}; \quad b(\delta) = \left(\frac{\omega}{2a} \right)^{1/2} \frac{\Gamma(\omega)}{\Gamma[\frac{1}{2}(1+\omega)]} \left(\frac{1+\delta}{\bar{\xi}_2^\delta} \right)^{(1-\omega)/2} \quad (\text{A10})$$

$$1 + \delta \gg \bar{\xi}_2^\delta; \quad p(\delta) = \frac{a_s}{(\bar{\xi}_2^\delta)^2} \left(\frac{1+\delta}{\bar{\xi}_2^\delta} \right) \exp \left(-\frac{1+\delta}{x_* \bar{\xi}_2^\delta} \right); \quad b(\delta) = -\frac{1}{\mathcal{G}'(\tau_s)} \frac{(1+\delta)}{\bar{\xi}_2^\delta} \quad (\text{A11})$$

The integral constraints satisfied by scaling function are $S_1 = \int_0^\infty x h(x) dx = 1$ and $S_2 = \int_0^\infty x^2 h(x) dx = 1$. These take care of normalization of the function $p(\delta)$. Similarly the normalization constraint over $b(\delta)$ can be expressed as $C_{11} = \int_0^\infty x b(x) h(x) dx = 1$, which translates into $\int_{-1}^\infty d\delta b(\delta) p(\delta) = 0$ and $\int_{-1}^\infty d\delta \delta b(\delta) p(\delta) = 1$. Several numerical studies have been conducted to study the behavior of $h(x)$ and $b(x)$ for different initial conditions see e.g. (Colombi, Bouchet & Hernquist 1996; Colombi, Bouchet & Schaeffer 1996; Colombi et al. 1997). For very small values of δ the behavior of $p(\delta)$ is determined by the asymptotic behavior of $\phi(z)$ for large values of y , and it is possible to define another scaling function $g(z)$ which is completely determined by ω , the scaling parameter can be expressed as $z' = (1 + \delta) a^{-1/(1-\omega)} (\bar{\xi}_2^\delta)^{\omega/(1-\omega)}$. However, numerically it is much simpler to determine ω from the study of $\sigma(y)$ compared to the study of $g(z)$.

$$1 + \delta \ll \bar{\xi}_2^\delta; \quad p(\delta) = a^{-1/(1-\omega)} (\bar{\xi}_2^\delta)^{\omega/(1-\omega)} \sqrt{\frac{(1-\omega)^{1/\omega}}{2\pi\omega z'^{(1+\omega)/\omega}}} \exp \left[-\omega \left(\frac{z'}{1-\omega} \right)^{-(1-\omega)/\omega} \right]; \quad b(\delta) = -\left(\frac{2\omega}{\bar{\xi}_2^\delta} \right)^{1/2} \left(\frac{1-\omega}{z'} \right)^{(1-\omega)/2\omega} \quad (\text{A12})$$

To summarize, we can say that the entire behavior of the PDF $p(\delta)$ is encoded in two different scaling functions, $h(x)$ and $g(z')$ and one can also study the scaling properties of $b(\delta)$ in terms of the scaling variables x and z in a very similar way.

A2.2 The Quasi-linear Regime

The first departure from Gaussianity can be studied analytically using perturbative techniques (Bernardeau 1992, 1994) as well as using steepest descent methods (Valageas 2000a,b, 2002). These techniques are also invaluable in modelling the statistics of extreme underdensities. The PDF and bias now can be expressed in terms of $G_\delta(\tau)$ (Bernardeau 1992, 1994):

$$p(\delta) d\delta = \frac{1}{-\mathcal{G}'_\delta(\tau)} \left[\frac{1 - \tau \mathcal{G}''_\delta(\tau)/\mathcal{G}'_\delta(\tau)}{2\pi \bar{\xi}_2^\delta} \right]^{1/2} \exp \left(-\frac{\tau^2}{2\bar{\xi}_2^\delta} \right) d\tau; \quad b(\delta) = -\left(\frac{k_a}{\bar{\xi}_2^\delta} \right) \left[(1 + \mathcal{G}_\delta(\tau))^{1/k_a} - 1 \right], \quad (\text{A13})$$

$$\mathcal{G}_\delta(\tau) = \mathcal{G}(\tau) - 1 = \delta. \quad (\text{A14})$$

The above expression is valid for $\delta < \delta_c$ where the δ_c is the value of δ which cancels the numerator of the pre-factor of the exponential function appearing in the above expression. For $\delta > \delta_c$ the PDF develops an exponential tail which is related to the presence of singularity in $\phi(z)$ in a very similar way as in the case of its highly non-linear counterpart (Bernardeau 1992, 1994):

$$p(\delta) d\delta = \frac{3a_s \sqrt{\bar{\xi}_2^\delta}}{4\sqrt{\pi}} \delta^{-5/2} \exp \left[-|z_s| \frac{\delta}{\bar{\xi}_2^\delta} + \frac{|\phi_s|}{\bar{\xi}_2^\delta} \right] d\delta; \quad b(\delta) = -\frac{1}{\mathcal{G}'(\tau_s)} \frac{(1+\delta)}{\bar{\xi}_2^\delta}. \quad (\text{A15})$$

The quasilinear regime remains relatively better understood than the highly nonlinear regime, as the connection to dynamics can be made using analytical schemes. Attempts have been made to extend the perturbative results to the highly nonlinear regime Colombi et al. (1997). The lower order cumulant correlators are related to the moments of the bias function. For the case of top-hat smoothing and spectral index n_e the lowest order of the cumulant correlator is given by (Bernardeau 1994): $C_{21}^{\eta\eta'} = 68/21 - (n_e + 3)/3$.

APPENDIX B: THE LOGNORMAL DISTRIBUTION

In addition to the hierarchical ansatz *lognormal* distribution too is a popular analytical model commonly used in cosmology (Hamilton 1985; Coles & Jones 1991; Bouchet et al 1993; Kofman et al. 1994; Bernardeau & Kofman 1995; Colombi 1994). It appears in the quasi-linear regime (Munshi, Sahni, Starobinsky 1994) as a natural outcome of gravitational dynamics, under certain simplifying assumptions (Matarresse et al. 1992). Lognormal distribution is routinely used to model the statistics of weak lensing observables (Munshi 2000; Taruya et al. 2002), clustering of Lyman- α absorption systems (e.g. Bi & Davidson (1997)) and more recently by (Munshi et al. 2011a) for modelling of the tSZ statistics.

To understand the construction of lognormal distribution, we introduce a Gaussian PDF in variable s : $p(s) = (2\pi\Xi)^{-1/2} \exp[-(s-\mu)^2/2\Xi]$. With a change of variable $s = \ln(r)$ we can write down the PDF of y which is a lognormal distribution $p(r) = (2\pi\Xi)^{-1/2} \exp[-(\ln(r) - \mu)^2/2\Xi]/r$. The extra factor of $(1/r)$ stems from the fact: $dr/r = ds$. Note that s is positive definite and is often associate with $\rho/\langle\rho\rangle = 1 + \delta$ which means $\langle r \rangle = 1$. The moment generating function for the lognormal terms of the mean μ and the variance Ξ has the following form: $\langle r^n \rangle = \exp(n\mu + n^2\Xi/2)$. This however leads to the fact that if the underlying distribution of r or the density is Gaussian we will have to impose the condition: $\mu = -\Xi/2$. In our notation above Ξ is the distribution of the underlying Gaussian field. The variance of r defined as $\langle r^2 \rangle - \langle r \rangle^2 = \exp(\Xi) - 1 = \xi_2^\delta$. So we can write $\Xi = \ln(1 + \xi_2^\delta)$. This is the result that was used above. The generalisation to two-point or bivariate PDF can be done following the same arguments and can be found in (Kayo, Taruya, Suto 2001).

In the limit of large separation $\Xi_{12} \rightarrow 0$ we can write down the two point PDF

$$p_{\ln}(\delta_1, \delta_2) = p_{\ln}(\delta_1)p_{\ln}(\delta_2)[1 + b_{\ln}(\delta_1)\xi_{12}^\delta b_{\ln}(\delta_2)]; \quad b_{\ln}(\delta_i) = \Lambda_i/\Xi. \quad (\text{B1})$$

However, it is simpler to estimate the cumulative or integrated bias associated with objects beyond a certain density threshold δ_0 . This is defined as $b(\delta > \delta_0) = \int_{\delta_0}^{\infty} p(\delta)b(\delta)d\delta / \int_{\delta_0}^{\infty} p(\delta)d\delta$. In the low variance limit $\xi_2^\delta \rightarrow 0$ the usual Gaussian result is restored $b(\delta) = \delta/\xi_2^\delta$. The parameters $\Lambda, \Lambda_i, \Xi_{12}, \Xi$ that we have introduced above can be expressed in terms of the two-point (non-linear) correlation function $\xi_{12}^\delta = \langle \delta_1 \delta_2 \rangle$ and ξ_2^δ is the volume average of the non-linear two-point correlation function ξ_{12} of the smoothed density field.

The validity and limitations of various aspects of the one-point and two-point PDFs have been studied extensively in the literature against N-body simulations Bernardeau (1992, 1994). It is known that in the weakly nonlinear regime the lognormal distribution is equivalent to the hierarchical model with a generating function $\mathcal{G}(\tau) = \exp(-\tau)$. This leads to $S_p = p^{p-2}$. The loop level corrections can be computed exactly for the lognormal distribution, which gives $S_3 = 3 + \xi_2^\delta$ and $S_4 = 16 + 15\xi_2^\delta + 6(\xi_2^\delta)^2 + (\xi_2^\delta)^3$. It has been shown (see e.g. Kayo, Taruya, Suto (2001)) that the lognormal distribution very accurately describes the cosmological distribution functions even in the nonlinear regime $\xi_2^\delta \leq 4$ for relatively high values of density contrast $\delta < 100$.